Major subject area: Biochemistry and Chemical Biology, Cell Biology

Edge-strand of BepA interacts with immature LptD on the β-barrel assembly machine to direct it to on- and off-pathways

Ryoji Miyazaki[1, 2], Tetsuro Watanabe[1], Kohei Yoshitani[1], Yoshinori Akiyama[1, *]

[1]Institute for Frontier Life and Medical Sciences, Kyoto University, Kyoto 606-8507, Japan

[2]Present address:

Division of Biological Science, Nara Institute of Science and Technology, Ikoma, Nara 630-0192, Japan

[*]Correspondence: yakiyama@infront.kyoto-u.ac.jp (Y. A.)

Abstract

The outer membrane (OM) of gram-negative bacteria functions as a selective permeability barrier. *Escherichia coli* periplasmic Zn-metallopeptidase BepA contributes to the maintenance of OM integrity through its involvement in the biogenesis and degradation of LptD, a β-barrel protein component of the lipopolysaccharide translocon. BepA either promotes the maturation of LptD when it is on the normal assembly pathway (on-pathway) or degrades it when its assembly is compromised (off-pathway). BepA performs these functions probably on the β-barrel assembly machinery (BAM) complex. However, how BepA recognizes and directs an immature LptD to different pathways remains unclear. Here, we explored the interactions among BepA, LptD, and the BAM complex. We found that the interaction of the BepA edge-strand located adjacent to the active site with LptD was crucial not only for proteolysis but also, unexpectedly, for assembly promotion of LptD. Site-directed crosslinking analyses indicated that the unstructured N-terminal half of the β-barrel-forming domain of an immature LptD contacts with the BepA edge-strand. Furthermore, the C-terminal region of the β-barrel-forming domain of the BepA-bound LptD intermediate interacted with a "seam" strand of BamA, suggesting that BepA recognized LptD assembling on the BAM complex. Our findings provide important insights into the functional mechanism of BepA.

Introduction

The cell envelope of diderm bacteria is composed of two membranes, namely the inner (cytoplasmic) membrane (IM) and the outer membrane (OM). The intermembrane space, known as periplasmic space, contains a peptidoglycan layer. The OM is the outermost layer of a cell directly facing the external milieu and acts as a selective permeability barrier that prevents the penetration of toxic compounds including antibiotics (Nikaido, 2003). The cell surface localization as well as the functional impotence of the OM make its components suitable drug targets.

Outer membrane proteins (OMPs), generally exhibiting a β-barrel fold formed by more than 8 β-strands, play important roles in maintaining the structural and functional integrity of the OM (Konovalova et al., 2017). Therefore, irregularities in OMP biogenesis result in elevated cellular sensitivity to toxic compounds (Hart et al., 2019; Oh et al., 2011). After synthesis in the cytoplasm and following translocation across the IM to the periplasm through the SecYEG translocon, OMPs are delivered to the OM by periplasmic chaperones such as DegP, Skp, and SurA, and are finally integrated into the OM (Konovalova et al., 2017; Plummer and Fleming, 2016; Ricci and Silhavy, 2019). The OM assembly of OMPs is mediated by the β-barrel assembly machinery (BAM) complex consisting of a β-barrel OMP, BamA, and four lipoproteins, namely BamB, BamC, BamD, and BamE (Plummer and Fleming, 2016; Ricci and Silhavy, 2019; Tomasek and Kahne, 2021). Among the BAM complex subunits, BamA and BamD are the only essential components, although recent studies have shown that certain BamA mutations render all other BAM subunits dispensable (Hart et al., 2020). The BAM complex has a silk-hat-like structure (Bakelar et al., 2016; Gu et al., 2016; Han et al., 2016; Iadanza et al., 2016; Tomasek et al., 2020); the OM-embedded C-terminal β-barrel domain of BamA forms the "crown" and the N-terminal periplasmic polypeptide transport-associated (POTRA) domains of BamA form the "brim" together with the BamB/C/D/E lipoproteins.

Lipopolysaccharide (LPS), another major OM constituent localized in the outer leaflet of the OM, is also important for the maintenance of the structure and function of the OM (Sperandeo et al., 2017). LPS is synthesized on the cytoplasmic side of the IM and flipped across the IM to the periplasm. After maturation, it is transported to the OM by the LPS transport (Lpt) proteins (Sperandeo et al., 2017). A heterodimer of LptD, a β-barrel OMP, and LptE, a lipoprotein, plays roles in the final step to insert LPS into the OM (Dong et al., 2014; Qiao et al., 2014; Wu et al., 2006). The OM assembly process of LptD is unique in that it is accompanied by

56 rearrangement of intramolecular disulfide bonds. The mature form of LptD possesses two disulfide bonds formed
57 by non-consecutive pairs of Cys residues (C31-C724 and C173-C725) (Ruiz et al., 2010). It has been shown,
58 however, that an assembly intermediate of LptD having disulfide bonds formed by consecutive pairs of the Cys
59 residues (C31-C173 and C724-C725) ($LptD^{C}$; LptD with **C**onsecutive disulfide bods) is first generated and
60 isomerized to $LptD^{NC}$ (LptD with **N**on-**C**onsecutive disulfide bods) during its assembly/maturation, which is
61 triggered by the association of LptD with LptE (Chng et al., 2012; Narita et al., 2013). The $LptD^{C}$ to $LptD^{NC}$
62 conversion should occur at a later step in the OM assembly because LptD presumably associates with LptE on the
63 BAM complex (Chimalakonda et al., 2011; Chng et al., 2012; Lee et al., 2016; Narita et al., 2013).

64 BepA (formally called YfgC), a bi-functional periplasmic protein that plays an important role in
65 maintaining OM integrity (Narita et al., 2013), belongs to the M48 family zinc metallopeptidases that include
66 prokaryotic and eukaryotic proteases (such as Ste24, Oma1, and HptX) involved in membrane quality control
67 (Rawlings et al., 2018).We have previously shown that BepA is involved in the biogenesis and quality control of
68 LptD. While BepA promotes the $LptD^{C}$ to $LptD^{NC}$ conversion (chaperone-like function) (Narita et al., 2013), it
69 also degrades the stalled or misassembled $LptD^{C}$ molecules that are generated due to an *lptD* mutation (*lptD4213*)
70 or decreased availability of or weakened interaction with LptE (protease function) (Narita et al., 2013; Soltes et
71 al., 2017). The BepA protein consists of an N-terminal M48 metallopeptidase domain and a C-terminal
72 tetratricopeptide repeat (TPR) domain that are associated closely to form a compact structure (**Figure 1A**) (Bryant
73 et al., 2021; Shahrizal et al., 2019). Our previous study suggested that the TPR domain of BepA directly interacts
74 with LptD and with the BAM complex with its TPR domain inserted into the interior of the periplasmic part (brim)
75 of the BAM complex (Daimon et al., 2017; Narita et al., 2013). A mutational study has suggested that these
76 interactions are important for BepA functions (Shahrizal et al., 2019). Recent studies have also shown that the His-
77 246 residue of BepA that coordinates the zinc ion at the proteolytic active site acts as an ON/OFF switch (His
78 switch) for the proteolytic activity of BepA (Bryant et al., 2021; Daimon et al., 2020). The dual functions of BepA
79 should be appropriately regulated because the unregulated expression of the proteolytic activity of BepA caused
80 by an H246 mutation leads to the degradation of the normally assembling LptD intermediate (Daimon et al., 2020).
81 However, information on the molecular mechanism of this regulation and the modes of the BepA–LptD interaction
82 in each BepA function remains elusive.

83 Here, we investigated the mechanism by which BepA established interaction with LptD in promotion
84 of its assembly and degradation. Our results showed that a conserved β-strand (edge-strand) located adjacent to
85 the BepA active site directly contacts with LptD and plays important roles in substrate proteolysis, like many other
86 proteases. In addition, we unexpectedly found that the edge-strand-mediated interaction with a substrate is also
87 required for the chaperone-like function of BepA, which should be enabled by the His switch-mediated repression
88 of the proteolytic activity. Crosslinking experiments demonstrated that BepA could interact with an LptD molecule
89 assembling on the BAM complex. Based on these observations, we propose a model explaining the edge-
90 strand/His switch-mediated functional regulation of BepA in LptD assembly/degradation.
91

Results

Interaction of the BepA edge-strand with LptD is crucial not only for proteolysis but also for assembly promotion of LptD by BepA

Zinc-metallopeptidases usually possess a β-strand, called edge-strand, located close to their proteolytic active sites (Akiyama et al., 2015; López-Pelegrín et al., 2013; Stöcker and Bode, 1995). While the edge-strand is known to play a critical role in substrate proteolysis by directly interacting with a substrate polypeptide by the strand addition mechanism and converts it into an extended conformation for its presentation to the active site and proteolysis, it has not been well-characterized in M48 proteases. The solved structures of *Escherichia coli* BepA (Bryant et al., 2021; Shahrizal et al., 2019) show that it has a β-strand (β2) that is conserved among the M48-peptidases and is located adjacent to the active site (**Figure1A** and **Figure 1-figure supplement 1**), suggesting that this strand presumably acts as an edge-strand. To examine the role of the β2 strand in BepA functions, we constructed BepA mutants by introducing Pro at each position in β2 (from Asn-105 to Phe-110; **Figure 1A**). We then investigated the effects of β2 mutations on the proteolytic activity of BepA against overproduced LptD. When LptD is overproduced from a multi-copy plasmid, it mainly accumulates in the form of $LptD^{C}$ possibly due to the limited availability of its partner protein, LptE (Daimon et al., 2020, 2017). This species probably represents a "normal" assembly intermediate as it is associated with the BAM complex (See below) and can be converted to the mature form ($LptD^{NC}$) when LptE is co-expressed (Miyazaki et al., 2018). As reported previously (Daimon et al., 2020, 2017), overproduced LptD was degraded by co-expressed wild-type BepA to generate discrete degradation products (**Figure 1B**). To examine the possible roles of the β2 strand in the function of BepA, we introduced a Pro substitution into the β2 strand, as a Pro residue would affect the secondary structure, and thus the function, of this strand. We found that the expression of a few BepA mutants (N105P, A106P, F107P, and A108P) led to a significantly decreased generation of the LptD degradation products (**Figure 1B**). These mutants accumulated at a level comparable to that of wild-type BepA, suggesting that they did not exert drastic effects on the overall structure of BepA. Furthermore, some of these mutations compromised the degradation of BamA in a Δ*surA* strain (Daimon et al., 2017) and the self-cleavage of BepA-His_{10} (BepA possessing a C-terminal His_{10}-tag) within the His_{10}-tag (Narita et al., 2013) (**Figure 1-figure supplement 2A** and **2B**). These results strongly suggest that the β2 strand is important for the proteolytic activity of BepA.

119 We next analyzed whether the β2 strand directly interacts with a substrate by using a site-directed *in*
120 *vivo* photo-crosslinking approach (Chin and Schultz, 2002; Miyazaki et al., 2020a). We expressed derivatives of
121 BepA-His_{10} harboring a photoreactive amino acid analog, *p*-benzoyl-L-phenylalanine (*p*BPA), at each position in
122 the β2 strand in a Δ*bepA* strain and examined their complementation activity regarding erythromycin (EM)
123 sensitivity of the cell and self-cleavage of BepA-His_{10}. The results showed that certain mutants (F107*p*BPA,
124 F109*p*BPA, and F110*p*BPA) were as functional as the wild-type, but others exhibited neither significant
125 complementation activity nor self-cleavage (**Figure 1-figure supplement 3A** and **3B**). For the photo-crosslinking
126 experiments conducted in this study, we used BepA variants harboring the E137Q mutation in the H^{136}ExxH motif
127 for two reasons. First, this mutation would repress the possible degradation of LptD by the BepA derivatives.
128 Second, our previous study has shown that this mutation stabilizes the interaction of BepA with LptD (Daimon et
129 al., 2017). Following UV irradiation of cells expressing each of the BepA mutants, BepA-His_{10} and its crosslinked
130 products were purified from the membrane fractions by affinity isolation using Ni-NTA agarose and subjected to
131 immunoblotting analysis (**Figure 1C**). The N105*p*BPA, A106*p*BPA, F107*p*BPA, and A108*p*BPA derivatives of
132 BepA generated, in a UV-dependent manner, evident crosslinked products that reacted with both anti-BepA and
133 anti-LptD antibodies. Taken together, these results imply that the β2 strand of BepA directly interacts with LptD
134 and plays an important role in their degradation. The structure, intramolecular disposition, as well as involvement
135 in substrate interaction and proteolysis of the β2 strand strongly supports the hypothesis that it indeed acts as the
136 edge-strand to recognize and present a substrate to the active site. We have thus referred to the β2 strand as "the
137 edge-strand" hereafter. BepA N105*p*BPA and F107*p*BPA derivatives also generated the unidentified crosslinked
138 products (**Figure 1C, open arrowheads**), suggesting that the edge strand would interact with some other substrates.
139 The differential effects of the mutations on the degradation of LptD and BamA and the self-cleavage of the C-
140 terminal tag (**Figure 1B** and **Figure 1-figure supplement 2A** and **2B**) might reflect their different interaction
141 properties and/or affinities for the BepA edge-strand. Our previous study also suggested substrate-specific
142 interaction of an edge-strand for another metallopeptidase, RseP (Akiyama et al., 2015).
143 BepA not only degrades the stalled or misassembled LptD (when LptD is on the normal (on-) pathway)
144 but also promotes the maturation of LptD through facilitating its assembly with the partner protein LptE
145 (chaperone-like activity) (on the off-pathway) (Narita et al., 2013). Therefore, we examined the effects of the edge-
146 strand Pro mutations on the chaperone-like activity of BepA. LptD possesses two intramolecular disulfide bonds.

147 While the mature (fully assembled) LptD has non-consecutive disulfide bonds, an assembly intermediate form of
148 LptD ($LptD^C$) that accumulates in the absence of functional BepA possesses consecutive disulfide bonds.
149 Consistent with our previous results (Narita et al., 2013), expression of the wild-type BepA in a Δ*bepA* strain
150 markedly decreased the accumulation of $LptD^C$. On the contrary, only a partial decrease in accumulation was
151 observed with the expression of the E137Q mutant. We found that the A106P mutant was defective in reducing
152 $LptD^C$ accumulation, suggesting that a mutation in the edge-strand could affect the chaperone-like function
153 (**Figure 1-figure supplement 4A**). Subsequently, we examined the effects of two edge-strand mutations—A106P
154 and F1107P—that markedly compromised LptD degradation on the chaperone-like function of BepA using pulse-
155 chase experiments. Expression of the wild-type BepA in Δ*bepA* cells significantly accelerated the conversion of
156 $LptD^C$ to $LptD^{NC}$, whereas expression of the protease-dead E137Q mutant demonstrated weakened conversion
157 (**Figure 1D**). The acceleration of the $LptD^C$ to $LptD^{NC}$ conversion by the F107P mutant was weaker than that by
158 the wild-type BepA (almost the same or slightly stronger as compared with the E137Q mutant), and no detectable
159 acceleration was observed with the A106P mutant (**Figure 1D**). These results unexpectedly revealed that the edge-
160 strand was also important for the chaperone-like activity of BepA.

161 BepA derivatives with a Cys substitution (note that BepA intrinsically does not possess a Cys residue),
162 instead of a Pro substitution, at the positions of Asn-105, Ala-106, or Phe-107 in the β2 strand exhibited almost
163 normal chaperone-like and proteolytic functions (**Figure 1-figure supplement 4B** and **4C**). This supports the idea
164 that the secondary structure of the edge-strand, but not the individual amino acid residues, is important for its
165 function. Note that, although it is possible that a Pro mutation also affects a local structure around the edge-strand,
166 the A106P mutant, which was defective in LptD and BamA degradation, still exhibited significant self-cleavage
167 of the probably unstructured C-terminal tag (**Figure 1-figure supplement 2B**), suggesting that this mutation, and
168 possibly the other Pro mutations, specifically affected the edge-strand structure, but not the active site or the
169 protein's overall structures.

170

171 **BepA interacts with the N-terminal half of the β-barrel-forming domain of the LptD assembly intermediate**

172 While BepA interacts with LptD to promote either its proper OM assembly or proteolytic elimination
173 depending on the situation (Narita et al., 2013), the details of the BepA–LptD interaction, including the region(s)
174 in LptD to which BepA binds, remain largely unknown. Thus, we performed a systematic photo-crosslinking

175 analysis to identify the BepA-contact region in the LptD assembly intermediate $LptD^C$. We performed photo-
176 crosslinking experiments in cells ectopically co-expressing an LptD derivative containing a photo-reactive amino
177 acid analog *p*BPA [LptD(*p*BPA)] and a protease-dead variant of BepA, BepA(E137Q). We first introduced *p*BPA
178 at each of the 50 positions (approximately every 15 residues) in the mature part of LptD and performed photo-
179 crosslinking analysis. Cells expressing LptD(*p*BPA)-His_{10} and BepA(E137Q) were grown and UV-irradiated, and
180 the total cellular proteins were analyzed by immunoblotting with anti-BepA and anti-His antibodies. Under this
181 condition, expressed LptD-His_{10} was considerably accumulated as $LptD^C$ (**Figure 2-figure supplement 1**)
182 irrespective of co-expression of BepA(E137Q). We detected clear crosslinking with BepA mainly in the N-
183 terminal half of the LptD β-barrel-forming domain (**Figure 2A**). We then performed a detailed photo-crosslinking
184 analysis for the 20 additional sites in the N-terminal half of the LptD β-barrel-forming domain (**Figure 2B**) and
185 found that BepA was crosslinked at several of these sites. The residues at the BepA-cross-linkable sites were
186 oriented both inward and outward in the mature LptD β-barrel (**Figure 2C** and **2D**). Moreover, the residue Gln-
187 393 at which the strongest crosslinking was observed was oriented inward. These results suggest that LptD while
188 interacting with BepA would not assume a higher-order structure like closed β-barrel (See Discussion). We
189 selected a few LptD(*p*BPA) derivatives that had been crosslinked with BepA as representatives and examined their
190 functionality. They supported the growth of LptD-depleted cells when expressed from a plasmid, indicating that
191 they were functional (**Figure 2-figure supplement 2**). The above-mentioned crosslinking results thus likely reflect
192 a functional interaction of LptD with BepA in the normal assembly pathway.
193
194 **BepA edge-strand directly interacts with the Tyr-331 residue in the β7 strand of the LptD β-barrel domain**
195 We investigated further to identify the region of LptD that interacts with the BepA edge-strand. First,
196 we examined the effects of the BepA edge-strand Pro mutations (F107P and A106P) on the LptD(*p*BPA)–BepA
197 crosslinking. The F107P mutation significantly decreased the efficiency of the crosslinking of BepA(N105*p*BPA)
198 and BepA(A106*p*BPA) with LptD (**Figure 3-figure supplement 1**). Additionally, the A106P mutation exhibited
199 a similar effect on the crosslinking of BepA(N105*p*BPA) with LptD. Based on these effects on crosslinking, we
200 inferred that these mutations affected the interaction of the edge-strand with LptD. Subsequently, we selected
201 several LptD(*p*BPA) derivatives that showed relatively strong crosslinking with BepA and examined the effect of
202 F107P and A106P mutations in the BepA edge-strand on the crosslinking of LptD(*p*BPA) with BepA. We found

203 that these mutations altered LptD–BepA crosslinking in a site-specific manner. Further, the amount of crosslinked
204 products markedly decreased for LptD(Y331*p*BPA), but not for other mutants (**Figure 3A**). These results strongly
205 suggest that the region around Tyr-331 in the β7 strand of the LptD β-barrel domain (**Figure 2D**) is crosslinked
206 with the edge-strand of BepA.

207 To further confirm the direct interaction of the BepA edge-strand with the LptD β7 strand, we
208 conducted site-specific disulfide crosslinking experiments. For this analysis, we used the above-described single
209 Cys derivatives of BepA harboring a Cys residue at the position of Asn-105, Ala-106, or Phe-107, and derivatives
210 of LptD having a Cys substitution at either of the six positions, including Tyr-331 at which introduction of *p*BPA
211 showed clear crosslinking with BepA (**Figure 3A**). The wild-type LptD protein harbors intrinsic four Cys residues
212 that form two disulfide bonds essential for the LptD function; therefore, each of these Cys-substituted LptD
213 mutants possessed five Cys residues in total. We confirmed that these Cys-substituted LptD derivatives
214 accumulated normally and retained their function (**Figure 3-figure supplement 2**). Cells expressing a combination
215 of BepA Cys mutants and LptD Cys mutants were grown, and total proteins were acid-denatured and dissolved in
216 SDS containing N-ethylmaleimide (NEM; NEM was included to block free Cys residues). Then, LptD-His_{10} and
217 its crosslinked products were affinity-isolated using the C-terminal His_{10}-tag, treated with or without 2-
218 mercaptoethanol (ME), and analyzed by SDS-PAGE and anti-BepA immunoblotting. We observed that certain
219 combinations of BepA and LptD derivatives showed a high-molecular-mass band in electrophoresis results.
220 Among them, the combination of BepA(N105C) and LptD(Y331C) showed the most intense band that exhibited
221 reaction with the anti-BepA antibody (**Figure 3B** and **Figure 3-figure supplement 2B**, no ME). These high-
222 molecular-mass bands were not observed with the wild-type LptD (no additional Cys) and disappeared upon
223 treatment with ME, suggesting that they were disulfide-crosslinked products (**Figure 3B** and **Figure 3-figure**
224 **supplement 2B**, + ME). These results are consistent with the photo-cross-linking experiments (**Figure 3A**) and
225 indicate that the edge-strand of BepA can directly bind to several regions in the N-terminal half of the LptD β-
226 barrel-forming domain, which includes the β7 strand containing Tyr-331.

227

228 **BepA interacts with an LptD intermediate associating with the seam region of BamA on the BAM complex**

229 We further investigated the mode of the interaction of the BepA-associated LptD with the BAM
230 complex. It has been recently shown that an assembly intermediate of LptD (LptD4213) interacts with the seam

231 region formed by the N- and C-terminal β-strands (β1 and β16, respectively) in the BamA barrel domain and forms
232 a hetero-complex, in which the C-terminal β-signal of the LptD4213was associated with the β1 strand of the BamA
233 seam (Lee et al., 2019). It has ben suggested that the interaction of the β-signal with the BamA β1 strand generally
234 facilitates the folding of the β-barrel domain of a substrate OMP (See **Figure 4D** and **5B)** (Tomasek and Kahne,
235 2021). We first examined the interaction of the BepA-associated LptD intermediate with BamA and BamD by
236 conducting *in vivo* photo-crosslinking experiments using the LptD derivatives with *p*BPA at the position of Glu-
237 749 or Tyr-726 in addition to the position of Tyr-331. *p*BPA at Glu-749 and Tyr-726 residue, both of which are
238 located near the β-signal of LptD, have been reported to be crosslinked with BamA and BamD, respectively, during
239 the LptD assembly (**Figure 4D**) (Lee et al., 2019, 2018). Complementation assay results showed that either of the
240 LptD derivatives containing one or two *p*BPA at Glu-749 and Tyr-726 were functional (**Figure 4-figure**
241 **supplement 1**). After UV-irradiation of the cells expressing LptD-His_{10} and the *p*BPA derivatives, LptD-His_{10} and
242 its crosslinked products were affinity-isolated from the membrane fractions and analyzed by immunoblotting. The
243 single *p*BPA derivatives indeed generated crosslinked products with the expected factors as: LptD(Y331*p*BPA)
244 with BepA, LptD(D749*p*BPA) with BamA, and LptD(Y726*p*BPA) with BamD (**Figure 4A** and **4B**). With the
245 double *p*BPA derivatives LptD(Y331/D749*p*BPA) and LptD(Y331/Y726*p*BPA), new crosslinked products with
246 higher molecular sizes were observed in addition to the ones observed with single *p*BPA mutants (**Figure 4A** and
247 **4B**). These results showed that the higher molecular-sized products represented BepA–LptD(Y331/D749*p*BPA)–
248 BamA and BepA–LptD(Y331/Y726*p*BPA)–BamD crosslinked products and that BepA interacts with an assembly
249 intermediate of LptD on the BAM complex.

250 We further conducted photo-crosslinking experiments using LptD locked on the BAM complex by
251 using an SH-crosslinker, 1,4-bismaleimidobutane (BMB). It has been previously shown (Lee et al., 2019) that a
252 cysteine placed near the N-terminal β-strand of the BamA β-barrel (S439C) was crosslinked with a cysteine
253 introduced near the β-signal of LptD (E733C) via BMB treatment (**Figure 4D**; **Figure 4-figure supplement 2A**).
254 We introduced a Y331*p*BPA mutation into LptD(E733C) and confirmed that the resultant mutant was functional
255 (Fig. S10*B*). When the LptD(Y331*p*BPA/E733C) mutant was expressed in a strain having a chromosomal
256 *bamA(S439C)* mutant gene, LptD–BepA crosslinked products were detected upon UV irradiation, whereas LptD–
257 BamA crosslinked products was detected upon BMB treatment. When cells were first treated with BMB and then
258 UV-irradiated, a higher mass product that reacted with both anti-BepA and anti-BamA antibodies was generated.

259 The generation of this product depended on both BMB-treatment and UV-irradiation (**Figure 4C**). These results
260 are fully consistent with the above photo-crosslinking results and further demonstrated that BepA could interact
261 with an LptD assembly intermediate associating with the seam site of BamA on the BAM complex.
262

263 **Discussion**

264 The involvement of BepA in the maintenance of structural and functional integrity of the OM was first
265 suggested on the basis of increased sensitivities of the Δ*bepA*(*yfgC*) strain to several antibiotics and chemicals,
266 which was similar to the characteristics of strains with a disruption of genes encoding proteins engaged in outer
267 membrane biogenesis (Narita et al., 2013; Ruiz et al., 2005; Tamae et al., 2008). We have previously shown that
268 BepA is involved in the biogenesis and quality control of LptD, probably on the BAM complex (Daimon et al.,
269 2020, 2017; Narita et al., 2013). However, the mechanism by which BepA recognizes and interacts with LptD
270 remains elusive. This information is important to understand the mechanism of BepA to distinguish between the
271 normal (on-) and off-pathway intermediates of LptD that are either assembled into the OM or degraded,
272 respectively. To gain insight into the BepA–LptD interaction, we examined the role of the conserved edge-strand
273 of BepA in its function. Our results showed that the BepA edge-strand participates not only in the proteolytic
274 activity but also, unexpectedly, in the chaperone-like activity through its direct interaction with LptD (**Figure 1**).
275 The results of the photo- and disulfide-crosslinking analyses indicated that the N-terminal half of the LptD β-
276 barrel-forming domain interacts with the BepA edge-strand (**Figure 2** and **Figure 3**). Moreover, we showed that
277 BepA demonstrated interaction with an LptD assembly intermediate whose C-terminal region was associated with
278 the seam strand of BamA on the BAM complex (**Figure 4**). These observations provide useful insights into the
279 BepA functions involved in the biogenesis and quality control of LptD.

280 Our previous results have shown that BepA interacts with the BAM complex via its C-terminal TPR
281 domain partly inserted into the periplasmic ring-like structure of the BAM complex (Daimon et al., 2017; Shahrizal
282 et al., 2019). In this study, we observed that BepA showed crosslinking with the N-terminal half of the LptD β-
283 barrel-forming domain but not with the C-terminal half. This observation was consistent with the localization of
284 LptD on the BAM complex; the N-terminal region was localized at/near the periplasmic surface of the BAM
285 complex, and the C-terminal region was inserted deep into the BAM complex's interior. The results of the Cys
286 crosslinking experiments showed that several positions, including Tyr-331, in the N-terminal half of the LptD β-
287 barrel-forming domain interacted with the edge-strand. The recently solved structures of BepA (Bryant et al.,
288 2021; Shahrizal et al., 2019) showed that the active site region including the edge-strand was located inside the
289 BepA molecule, leading to the suggestion that structural changes in BepA including the movement of the α6 and
290 α9 loops covering the active site/edge-strand were necessary to enable access of a substrate to the active site/edge-

291 strand region (**Figure 5-figure supplement 1**). However, even after such structural changes, the edge-strand
292 should be located at a recessed position. This suggests that the regions around the BepA-crosslinked positions in
293 the LptD assembly intermediate do not form an extensive β-sheet structure as found in the mature LptD to gain
294 access to the edge-strand of BepA (**Figure 5-figure supplement 1**). Furthermore, *p*BPA at positions of both the
295 inward-pointing and outward-pointing residues in the mature β-barrel domain of LptD was crosslinked with BepA.
296 Collectively, these results support the hypothesis that the BepA-interacting region of the LptD intermediate is
297 largely unstructured. The unstructured nature of these proteins is in fact helpful to accommodate in or around the
298 narrow space inside the BAM complex. The TPR domain of BepA has also been shown to contact with LptD to
299 promote its biogenesis and degradation (Daimon et al., 2017). Currently, we have no information available on the
300 part of LptD that interacts with the TPR domain. The TPR domain may act either together with the edge-strand at
301 the same step or independently at other steps during LptD assembly and degradation.

302 Further, our results suggest that the proper interaction of LptD with the edge-strand of BepA is
303 important for the promotion of its assembly as well as degradation by BepA (**Figure 1** and **Figure 5A**). This
304 finding was unexpected as it raised a question of how the degradation of the normally assembling LptD
305 intermediate can be avoided despite its interaction with the edge-strand near the protease active site. In the BepA
306 structures, the conserved His-246 residue is coordinated to a zinc ion in the active site to block the activation of a
307 water molecule necessary for the catalysis of the proteolytic reaction (Bryant et al., 2021; Shahrizal et al., 2019).
308 We have recently reported that His-246 acts as a switch to regulate the proteolytic activity of BepA (Daimon et
309 al., 2020). This His-Switch-mediated repression of the protease activity would enable the interaction of LptD
310 intermediates at the protease active site of BepA without degradation. Indeed, the derepressed BepA(H246A)
311 mutant degrades an LptD intermediate on the normal assembly pathway, instead of promoting its biogenesis
312 (Daimon et al., 2020). One possible model for the discrimination of LptD intermediates by BepA for assembly or
313 degradation would be as follows (**Figure 5A**). In both assembly and degradation pathways of LptD, an unknown
314 signal(s), such as a specific interaction of BepA with the substrate and/or the BAM complex, induces a structural
315 change in BepA (dislocation of the α6 loop covering the active site) to expose its active site and to enable the
316 interaction between the LptD polypeptide and the edge-strand, whereas His-246 continues to repress the
317 degradation of LptD by BepA. This interaction is necessary for both proper assembly and degradation of LptD.
318 The transient interaction of normally assembling LptD with the "protease activity-repressed" state of BepA would

319 provide sufficient time for the progression of the maturation processes of LptD (including association with LptE),
320 resulting in the final release of mature LptD from BamA. In contrast, during the prolonged stay of stalled or
321 misassembled LptD molecules, BepA undergoes a further structural change including the movement of the α9
322 loop, stochastically or induced by a specific signal(s), to remove His-246 from the active site zinc, leading to the
323 degradation of the molecules that cannot be subjected to maturation successfully. Our previous results of pulse-
324 chase experiments showed that, although the conversion of $LptD^{C}$ to $LptD^{NC}$ was relatively slow, it started
325 immediately after the synthesis of LptD and proceeded rather constantly (Narita et al., 2013). In contrast,
326 degradation of stalled LptD in an LptE-depleted strain apparently occurred in a biphasic manner; little degradation
327 of stalled LptD was observed for several minutes after synthesis ((Narita et al., 2013), indicating the presence of
328 a lag period for degradation of stalled LptD to occur. These observations are consistent with the above model.
329 Notably, it has been reported that BepA expression can result in the degradation of a mutant form of LptD
330 (LptD4213) that probably mimics a late-state assembly intermediate of LptD (Lee et al., 2016) and possesses a
331 substantial degree of a higher order (β-barrel-like) structure. The mechanism by which LptD4213 is degraded by
332 BepA remains unclear, but its N-terminal region may interact with BepA.

333 BepA possibly facilitates the association of LptD with LptE on the BAM complex as the phenotypes
334 caused by the disruption of BepA, including drug sensitivity and retarded disulfide rearrangement in LptD, can be
335 suppressed by the overproduction of LptE (Narita et al., 2013). We have previously detected two species of $LptD^{C}$;
336 one is not associated with LptE and observed only in an extremely early phase of its membrane assembly, and the
337 other is associated with LptE and formed at a later phase (Miyazaki et al., 2018). It is likely that the $LptD^{C}$ molecule
338 that was simultaneously crosslinked with BepA and BamA was not associated with LptE, as it was accumulated
339 in the LptE-limiting condition; therefore, it would represent the former species of $LptD^{C}$ mentioned above. We
340 assume that this LptD intermediate may possess a partially folded structure in which the BamA-associating C-
341 terminal region of the barrel domain has a certain degree of a higher order (β-sheet) structure, but the BepA-
342 associating N-terminal region is largely unstructured. Such a state of LptD may be favorable for the association of
343 LptE with LptD (**Figure 4D**). Interestingly, Tyr-331 of LptD that contacts with the edge-strand of BepA is located
344 at the end of the LptE-surrounding region of the LptD β-barrel in the mature LptD/E complex (**Figure 2D**). The
345 interaction with the edge-strand of BepA may pin the partially folded structure of LptD transiently and facilitate
346 the association between LptD and LptE. It might also assist the formation of the β-sheet structure in the β barrel

347 forming domain of LptD. Although it is possible that BepA actively promotes the LptD–LptE association by
348 interacting with both LptD and LptE, it is also possible that BepA plays a passive role by maintaining an
349 appropriate structure of LptD for association with LptE without showing direct interaction with LptE.

350 The biogenesis of LptD has been well studied. LptD has been a focus of OM protein research because
351 it provides important information on its essential cellular function and it can be used as a model for OM protein
352 insertion into the OM by the BAM complex. Based on the results obtained in the previous and current studies, we
353 propose a model of the BepA-assisted biogenesis of LptD (**Figure 5B**): (i) After synthesis in the cytoplasm, LptD
354 is translocated to the periplasm through the SecYEG translocon, during or just after which the Cys residues are
355 oxidized by DsbA to form $LptD^{C}$ (Chng et al., 2012; Narita et al., 2013). It is then targeted to the BAM complex
356 with the aid of periplasmic chaperones including SurA (Schwalm et al., 2013; Vertommen et al., 2009); (ii) The
357 C-terminal β-signal region of LptD is inserted into the BAM complex possibly through the periplasmic ring-like
358 structure formed by the BamA POTRA domains and the lipoprotein subunits of the BAM complex, and it
359 establishes interaction with BamD and BamA (Lee et al., 2019); (iii) Although details of the exact juncture at
360 which interaction occurs are unknown, BepA interacts with the largely unstructured N-terminal half of the LptD
361 β-barrel-forming domain whose C-terminal β-signal region is associated with the seam region of BamA. This
362 helps the association of LptE with LptD; (iv) Then, the folding (β-sheet formation) of the unstructured N-terminal
363 region of the LptD β-barrel domain occurs to form a premature form of LptD with a substantially folded β-barrel
364 domain and LptE within it, like LptD4213 (Lee et al., 2019, 2016); (v) The β-barrel domain of LptD β-barrel is
365 finally released from BamA and closed to form the mature LptD/E complex. The isomerization of two disulfide
366 bonds in LptD ($LptD^{C}$ to $LptD^{NC}$) should occur at a later step after the association of LptD and LptE (Lee et al.,
367 2016; Miyazaki et al., 2018). The LptD intermediates that are stalled at certain steps in the above-mentioned
368 processes as a result of misfolding are eliminated by the action of several peptidases including DegP (in the
369 periplasm) and BepA /YcaL (on the BAM complex) (Soltes et al., 2017).

370 Our study reports several new findings on the interaction of BepA with LptD and BamA on the BAM
371 complex where BepA plays a crucial role in the biogenesis and degradation of LptD. Further, we proposed a model
372 explaining the role of BepA in these processes. Nonetheless, there are many questions that warrant further
373 investigation. It would be especially important to elucidate the mechanism by which the substrate gains access to
374 the active site buried inside the BepA molecule and the manner in which the switching of BepA from the state

375 with chaperone-like function to that with protease function occurs. The possible movement of the α6 and α9 loops
376 should be directly examined. It is possible that there are signals that arise from the BAM complex and/or from
377 (stalled) LptD to induce this structural/functional conversion of BepA. Further study, including structural and
378 biochemical analysis of the BepA–LptD–BAM complex, is necessary to substantiate our model and to elucidate
379 the molecular details of BepA functions. Cell surface proteins are suitable drug targets as they are more easily
380 accessible from the external milieu than cytoplasmic proteins. These studies can provide a basis for the
381 development of new drugs targeted to BepA/LptD/BAM.

382 ## Materials and methods

383 **Key resources table**

Reagent type or resource	Designation	Source reference	Identifiers	Additional information
Strains	*E. coli*	This study	N/A	Supplementary file 1
Virus	P1 bacteriophage	Laboratory stock	CGSC12133	
Recombinant DNA	Plasmids	This study	N/A	Supplementary file 2
Oligonucleotides		This study	PCR primers	described in the below
Antibodies	1st antibodies	This study	N/A	listed in the below
Antibody	Goat Anti-Rabbit IgG (H + L)-HRP Conjugate	Bio-Rad Laboratories	1706515	
Chemical compound	H-p-Bz-Phe-OH	Bachem	F2800	
Chemical compound	Methionine, L-[^{35}S] Translation Grade	American Radiolabeled Chemicals	ARS 01014	
Chemical compound	nProtein A Sepharose™ 4 Fast Flow	GE Healthcare	17528004	
Chemical compound	Ni-NTA Agarose	QIAGEN	30250	
Critical Commercial Assays	ECL™ Western Blotting Detection Reagents	GE Healthcare	RPN2106	
Critical Commercial Assays	ECL™ Prime Western Blotting Detection Reagents	GE Healthcare	RPN2232	
Software, Algorithm	Microsoft Excel	Microsoft	N/A	
Software, Algorithm	Bio-imaging Analyzer BAS-1800, BAS-5000	Fujifilm/GE Healthcare	N/A	
Software, Algorithm	Image Qaunt LAS 4000 mini	Fujifilm/GE Healthcare	N/A	
Software, Algorithm	Multi Gauge	Fujifilm/GE Healthcare	N/A	

384

385 **Bacterial strains, Plasmids and Primers**

386 *Escherichia coli* K12 strains and plasmids used in this study are listed in Tables S1 and S2, respectively. Details
387 of the strain and plasmid construction and media are described in Construction of Mutant Strains and Plasmids
388 Construction, respectively.

389

390 **Media and Bacterial Cultures**

391 *E. coli* cells were grown in L rich medium (10 g/L bacto-tryptone, 5 g/L bacto-yeast extract, 5 g/L NaCl; pH
392 adjusted to 7.2 with NaOH) or M9 synthetic medium (without $CaCl_2$; (Miller, 1972)) supplemented with maltose
393 (final 0.2%), glycerol (final 0.4%), all amino acids (except Met and Cys; final concentration of 20 μg/mL each).
394 50 μg/mL ampicillin (Amp), 20 μg/mL chloramphenicol (Cm), 25 μg/mL kanamycin (Km), 25 μg/mL tetracycline
395 (Tet) and 50 μg/mL spectinomycin (Spc) were added as appropriate for growing plasmid-bearing cells and
396 selection of transformants and transductants. Bacterial growth was monitored with Mini photo 518R (660 nm;
397 TAITEC Co., Saitama, Japan).
398
399 **Antibodies**
400 Penta-His HRP conjugate was purchased from QIAGEN (Hilden, Germany). Anti-BepA (Narita et al., 2013), anti-
401 LptD (Narita et al., 2013) and anti-BamA (Gunasinghe et al., 2018) antibodies were described previously.
402
403 **Construction of Mutant Strains**
404 RM2091 (JE6631, *purC80*::Tn*10*) was constructed by transferring the *purC80*::Tn*10* marker, which is located
405 near the *bepA* gene, from CAG18470 (Nichols et al., 1998) into JE6631 (Miyazaki et al., 2018), respectively, by
406 P1 transduction. RM2243 (AD16, *bepA(E137Q) purC80*::Tn*10*) was constructed as follows. pRM330 (a plasmid
407 carrying *bepA(E137Q)*, see below) was introduced into RM2091 to yield cells with pRM330 integrated into the
408 chromosome by homologous recombination in the *bepA* region. They were then grown on an L-agar plate
409 containing 5% sucrose to select cells that had lost the integrated plasmid. The plasmid-cured cells were screened
410 for those having the chromosomal *bepA(E137Q)* allele at the *bepA* locus. The *bepA(E137Q)* allele was finally
411 transferred to AD16 (Kihara et al., 1995) by joint P1 transduction with the *purC80*::Tn*10* marker. One of such
412 strains was named RM2243. RM3654 (AD16, Δ*bepA*, *bamA*$^+$ *zae502*::Tn*10*) and RM3655 (AD16, *bamA(S439C)*
413 *zae502*::Tn*10*) were constructed as follows, pRM845 (a plasmid carrying *bamA(S439C)*, see below) was
414 introduced into YH188 (JE6631, *zae502*::Tn*10*) (Hizukuri and Akiyama, 2012) to yield cells with pRM845
415 integrated into the chromosome by homologous recombination in the *bamA* region. They were then grown on an
416 L-agar plate containing 5% sucrose to select cells that had lost the integrated plasmid. The plasmid-cured cells
417 were screened for those having the chromosomal *bamA(S439C)* allele at the *bamA* locus. The *bamA(S439C)* allele
418 was transferred to SN56 (Narita et al., 2013) by joint P1 transduction with the *zae502*::Tn*10* marker. Strains having

419 the *bamA*$^{+}$ allele and the *bamA(S439C)* allele were picked up and named RM3654 and RM3655, respectively.
420 RM2831 (HM1742, *kan araC*-P$_{araBAD}$-*lptD*) were constructed by essentially the same procedure as the construction
421 of strains with a chromosomal C-terminal his$_{10}$-tagged gene (Miyazaki et al., 2020b). First, a *kan araC*-P$_{araBAD}$-
422 *lptD* fragment having a sequence identical to the upstream or downstream region of the *lptD* start codon at the
423 respective ends of the fragment, was PCR-amplified from pRM741 (a plasmid carrying a *kan* cassette at the
424 upstream of an *araC*-P$_{araBAD}$) using a pair of primers, ara-lptD-f (5'-
425 TTGTCACGCGCAACGTTACCGATGATGGAACAATAAAATCAACGTCATATGAATATCCTCCTTAG-
426 3') and ara-lptD-r (5'-
427 GGTGGCAATCATGGTGGCCAGGAGAGTGGGGATACGTTTTTTCATGGTGAATTCCTCCTGCTAG-3').
428 Then, the chromosomal *lptD* locus of the *E. coli* DY330 strain was replaced by this fragment using the λ-Red
429 recombination system (Yu et al., 2000). The *kan araC*-P$_{araBAD}$-*lptD* was finally transferred to HM1742 by P1
430 transduction.
431
432 **Plasmids Construction**
433 pSTD689-derived plasmids carrying a *bepA* mutants were constructed from pRM290 (pSTD689-*bepA*) (Daimon
434 et al., 2017) by site-directed mutagenesis. Derivatives of pRM291 (pSTD689-*bepA(E137Q)*) (Daimon et al., 2017)
435 carrying an additional Cys mutation and derivatives of pUC-*bepA(E137Q)-his$_{10}$* (pUC18-*bepA(E137Q)-his$_{10}$*)
436 (Narita et al., 2013) carrying an *amber* mutation were constructed by site-directed mutagenesis. pUC18-
437 *bepA(Pro)-his$_{10}$* and pUC18-*bepA(amb)-his$_{10}$* plasmids were constructed from pUC-*bepA-his$_{10}$* (pUC18-*bepA-*
438 *his$_{10}$*) (Narita et al., 2013) by site-directed mutagenesis. To construct pUC18-*bepA(Pro, amb, E137Q)-his$_{10}$*
439 plasmids, a mutation for the individual Pro substitutions was introduced into each of the pUC18-*bepA(amb,*
440 *E137Q)-his$_{10}$* plasmids by site-directed mutagenesis. pNB91 (pMW118-*bepA(E137Q)*) was constructed by
441 subcloning an EcoRI-HindIII *bepA(E137Q)* fragment prepared from pUC-*bepA(E137Q)* (pUC18-*bepA(E137Q)*)
442 (Narita et al., 2013) into the same sites of pMW118. pRM807 (pMW118-*bepA(A106P, E137Q)*) and pRM808
443 (pMW118-*bepA(F107P, E137Q)*) were also constructed by subcloning an EcoRI-HindIII *bepA* fragment from
444 each of pSTD639-*bepA* plasmids into the same sites of pMW118.
445 Plasmids carrying *lptD(amb)-his$_{10}$* were constructed from pRM309 (pRM294-*lptD-his$_{10}$*) (Miyazaki
446 et al., 2018) by site-directed mutagenesis. pRM821 (pRM294-*lptD(Y331amb, D749amb)-his$_{10}$*) and pRM822

447 (pRM294-*lptD(Y331amb, Y726amb)-his*$_{10}$) were constructed from pRM626 (pRM294-*lptD(Y331amb)-his*$_{10}$) by
448 site-directed mutagenesis. pRM829 (pRM294-*lptD(E733C)-his*$_{10}$) and pRM831 (pRM294-*lptD(Y331, E733C)-*
449 *his*$_{10}$) were constructed from pRM309 and pRM626, respectively, by site-directed mutagenesis. Plasmid carrying
450 *lptD(Cys)-his*$_{10}$ were constructed as follows. Each mutation for the Cys substitutions was introduced to pRM309
451 by site-directed mutagenesis. The BamHI-HindIII *lptD(Cys)-his*$_{10}$ fragment of the resulting plasmids was
452 subcloned into the same site of pTWV228 (Takara Bio inc., Shiga, Japan) to generate pTWV228- *lptD(Cys)-his*$_{10}$.
453 pRM320 (pUC118-*bepA-yfgD*) was constructed by PCR amplification of the *bepA-yfgD* fragment
454 from the genome of MC4100 using a pair of primers, bepA-f (5'-
455 GCGCGCGGATCCATTTGAGTGGGCTAATCTTCG-3') and yfgD-r (5'-
456 GCGCGCGTCGACCGAACTACGCGAAGTTAATCC-3'), and, cloning it into the BamHI-SalI site of pUC118
457 (Takara Bio) after digestion with these enzymes. For the construction of pRM324, the *bepA(E137Q)* mutation was
458 introduced into pRM320 by site-directed mutagenesis. pRM330 (pK18mobsacB-*bepA(E137Q)-yfgD*) was
459 constructed by subcloning the BamHI-SalI *bepA(E137Q)-yfgD* fragment from pRM324 into the same sites of
460 pK18mobsacB (Schäfer et al., 1994).
461 pRM823 (pUC118-*bamA*) was constructed by *in vitro* recombination using In-Fusion HD cloning kit
462 (Takara Bio) of a EcoRI-BamHI fragment from pUC118 and a *bamA* fragment prepared by PCR amplification
463 from the genome of MC4100 using a pair of primers, bamA-f (5'-
464 GCGCGAATTCAGGAAGAACGCATAATAACG-3') and bamA-r (5'-
465 GCGCGGATCCTTACCAGGTTTTACCGATG-3'). For the construction of pRM836, the *bamA(S439C)*
466 mutation was introduced into pRM823 by site-directed mutagenesis. pRM845 (pK18mobsacB-*bamA(S439C)*) was
467 constructed by subcloning the EcoRI-BamHI *bamA(S439C)* fragment from pRM823 into the same sites of
468 pK18mobsacB.
469
470 **Immunoblotting analysis**
471 Acid-denatured proteins were solubilized in SDS-sample buffer (62.5 mM Tris-HCl (pH 6.8), 2% SDS, 10%
472 glycerol, 5 mg/mL bromophenol blue) with or without 10% β-ME, separated by SDS-PAGE and electro-blotted
473 onto a PVDF membrane (Merck Millipore; Billerica, MA). The membrane was first blocked with 5% skim milk
474 in PBST (Phosphate Buffered Saline with Tween 20), and then incubated with Penta-His HRP conjugate (1/2,000

475 or 1/3,000 dilution)), anti-BepA (1/10,000), anti-LptD (1/50,000) or anti-BamA (1/20,000). After washing with
476 PBST, the membrane was incubated with a horseradish peroxidase (HRP)-conjugated secondary antibody
477 (1/5,000) (Goat Anti-Rabbit IgG (H + L)-HRP Conjugate; Bio-Rad Laboratories, Inc., Hercules, CA) in PBST
478 (This step was omitted for the detection using Penta-His HRP conjugate). Proteins were visualized with ECL™
479 Western Blotting Detection Reagents (GE Healthcare UK Ltd, *Amersham Place* Little Chalfont, England) or
480 ECL™ Prime Western Blotting Detection Reagents (GE Healthcare) and LAS4000 mini lumino-image analyzer
481 (GE Healthcare).
482
483 **Pulse-chase analysis for assay of the LptD disulfide-isomerization**
484 Cells were first grown at 30°C in M9-medium supplemented with 2 μg/mL thiamine, 0.4% glycerol, 0.2% maltose,
485 all amino acids (except Met and Cys) with or without 0.05% arabinose until early log phase. After induction with
486 1 mM IPTG for 15 min, cells were pulse-labeled with 370 kBq/mL [^{35}S]Methionine for 1 min. At appropriate time
487 points after addition of excess nonradioactive Met (final conc. 250 μg/mL), total cellular proteins were precipitated
488 with 5% TCA, washed with acetone, solubilized in SDS-buffer (50 mM Tris-HCl (pH 8.1), 1% SDS, 1 mM EDTA)
489 and diluted 33-fold with Triton-buffer (50 mM Tris-HCl (pH 8.1), 150 mM NaCl, 2% Triton X-100, 0.1 mM
490 EDTA). After clarification, samples were incubated with anti-LptD antibodies and nProtein A Sepharose™ 4 Fast
491 Flow (GE healthcare) at 4ºC over-night with slow rotation. Proteins bound to the antibody/ProteinA-Sepharose
492 were recovered by centrifugation, washed with Triton buffer and then with 10 mM Tris-HCl (pH 8.1) and eluted
493 by incubation at 98°C for more than 5 min in SDS-sample buffer. The samples were divided into two portions and
494 one was treated with 10% β-ME. The proteins were separated by SDS-PAGE, and visualized with BAS1800
495 phosphoimager. Relative $LptD^{NC}$ were calculated by the following equation: Relative $LptD^{NC}$ = [$LptD^{NC}_{(X}$
496 $_{min)}$]/[$LptD^{C}_{(X\ min)}$ + $LptD^{NC}_{(X\ min)}$], where $LptD^{NC}$ and $LptD^{C}$ are the intensities of the respective bands.
497
498 ***In vivo* photo-crosslinking analysis**
499 For the experiments in Figure 1D and Figure 3-figure supplement 1, cells were grown at 30°C in L medium
500 containing 0.5 mM *p*BPA and 0.02% arabinose until early log phase and induced with 1 mM IPTG for 1 h. A half
501 volume of the cell cultures was put on a petri dish and UV-irradiated at 4ºC for 10 min using B-100AP UV lamp
502 (365 nm; UVP, LLC., Upland, CA), at the distance of 4 cm. The other half was kept on ice as non-UV-irradiated

503 samples. Membrane fractions were prepared by sonical cell disruption and the following ultracentrifugation, and
504 solubilized with SDS-buffer (50 mM Tris-HCl (pH 8.1), 1% SDS, 1 mM EDTA). After 33-fold diluted with Triton-
505 buffer (50 mM Tris-HCl (pH 8.1), 150 mM NaCl, 2% Triton X-100, 0.1 mM EDTA) and clarification, samples
506 were subjected to pull-down with Ni-NTA Agarose (QIAGEN). The isolated proteins were solubilized in SDS-
507 sample buffer (62.5 mM Tris-HCl (pH 6.8), 2% SDS, 10% glycerol, 5 mg/mL bromophenol blue) containing ME
508 and analyzed by SDS-PAGE and immunoblotting analysis.

509 For the experiments in Figure 2A, 2B and 3A, cells were grown at 30°C in L medium containing 0.5
510 mM *p*BPA and 0.02% arabinose until early log phase and induced with 1 mM IPTG for 3 h. While a half volume
511 of the cell cultures was UV-irradiated for 10 min, the other half was kept on ice as non-UV-irradiated samples, as
512 above. Total cellular proteins were precipitated with 5% TCA, washed with acetone, and solubilized in SDS-
513 sample buffer containing ME. The samples were subjected to SDS-PAGE and immunoblotting analysis.

514 For experiments in Figure 4A and 4B, cells were grown at 30°C in L medium containing 0.5 mM
515 *p*BPA and 0.02% arabinose until early log phase and induced with 1 mM IPTG for 3 h. While a half volume of
516 the cell cultures was UV-irradiated for 10 min, the other half was kept on ice as non-UV-irradiated samples, as
517 above. Membrane fractions were prepared as above and solubilized in SDS-buffer. After dilution with Triton-
518 buffer and clarification, samples were subjected to pull-down with Ni-NTA Agarose. The isolated proteins were
519 solubilized in SDS-sample buffer containing ME and analyzed by SDS-PAGE and immunoblotting analysis.

520

521 **BMB crosslinking combined with photo-crosslinking**

522 Cells were grown at 30°C in L medium containing 0.5 mM *p*BPA and 0.02% arabinose until early log phase and
523 induced with 1 mM IPTG for 3 h. BMB crosslinking was performed essentially according to the previously
524 described procedures (Lee et al., 2019). After quenching the BMB crosslinking, cells were treated with or without
525 UV-irradiation for 30 min at 4ºC. Total cellular proteins were precipitated with 5% TCA, washed with acetone,
526 and suspended in SDS-sample buffer containing 12.5 mM NEM for blocking the free Cys residues. After dilution
527 with Triton-buffer and clarification, samples were subjected to pull-down with Ni-NTA Agarose. The isolated
528 proteins were suspended in SDS-sample buffer containing ME and analyzed by SDS-PAGE and immunoblotting
529 analysis.

530 **Article and author information**

531 **Author details**

532 **Ryoji Miyazaki**

533 Institute for Frontier Life and Medical Sciences, Kyoto University, Kyoto, Japan

534 **Contribution:** Conceptualization, Methodology, Investigation, Resources, Writing–Original Draft, Writing–

535 Review & Editing and Funding Acquisition

536 **Competing interests:** No competing interests declared

537 **ORCID:** 0000-0003-1626-2569

538

539 **Tetsuro Watanabe**

540 Institute for Frontier Life and Medical Sciences, Kyoto University, Kyoto, Japan

541 **Contribution:** Methodology, Investigation, Resources

542 **Competing interests:** No competing interests declared

543 **ORCID:**

544

545 **Kohei Yoshitani**

546 Institute for Frontier Life and Medical Sciences, Kyoto University, Kyoto, Japan

547 **Contribution:** Resources

548 **Competing interests:** No competing interests declared

549 **ORCID:**

550

551 **Yoshinori Akiyama**

552 Institute for Frontier Life and Medical Sciences, Kyoto University, Kyoto, Japan

553 **Contribution:** Writing–Original Draft, Writing–Review & Editing, Supervision and Funding Acquisition

554 **Competing interests:** No competing interests declared

555 **ORCID:** 0000-0003-4483-5408

Funding

This work was supported by the Japan Society for the Promotion of Science KAKENHI Grants 18H06047, 19K21179 and 20K15715 (to R.M.), and 15H01532 and 18H023404 (to Y.A.), and research grants from the Institute for Fermentation Y-2020-02-027 (to R.M.). and from the Nagase Science and Technology Foundation (to Y.A.).

Acknowledgments

We thank our laboratory members and S. Narita for discussion and helpful advices.

564 **References**

565 Akiyama K, Mizuno S, Hizukuri Y, Mori H, Nogi T, Akiyama Y. 2015. Roles of the membrane-reentrant β-
566 hairpin-like loop of RseP protease in selective substrate cleavage. *eLife* **4**:e08928. doi:10.7554/eLife.08928

567 Bakelar J, Buchanan SK, Noinaj N. 2016. The structure of the β-barrel assembly machinery complex. *Science*
568 **351**:180–186. doi:10.1126/science.aad3460

569 Bryant JA, Cadby IT, Chong ZS, Boelter G, Sevastsyanovich YR, Morris FC, Cunningham AF, Kritikos G, Meek
570 RW, Banzhaf M, Chng SS, Lovering AL, Henderson IR. 2021. Structure-function characterization of the
571 conserved regulatory mechanism of the *Escherichia coli* M48 metalloprotease BepA. *J Bacteriol*
572 **203**:e00434-20. doi:10.1128/JB.00434-20

573 Chimalakonda G, Ruiz N, Chng S-S, Garner RA, Kahne D, Silhavy TJ. 2011. Lipoprotein LptE is required for the
574 assembly of LptD by the β-barrel assembly machine in the outer membrane of *Escherichia coli*. *Proc Natl*
575 *Acad Sci U S A* **108**:2492–2497. doi:10.1073/pnas.1019089108

576 Chin JW, Schultz PG. 2002. In vivo photocrosslinking with unnatural amino acid mutagenesis. *ChemBioChem*
577 **3**:1135–1137. doi:10.1002/1439-7633(20021104)3:11<1135::AID-CBIC1135>3.0.CO;2-M

578 Chng SS, Xue M, Garner RA, Kadokura H, Boyd D, Beckwith J, Kahne D. 2012. Disulfide rearrangement
579 triggered by translocon assembly controls lipopolysaccharide export. *Science* **337**:1665–1668.
580 doi:10.1126/science.1227215

581 Daimon Y, Iwama-Masui C, Tanaka Y, Shiota T, Suzuki T, Miyazaki R, Sakurada H, Lithgow T, Dohmae N,
582 Mori H, Tsukazaki T, Narita S-I, Akiyama Y. 2017. The TPR domain of BepA is required for productive
583 interaction with substrate proteins and the β-barrel assembly machinery complex. *Mol Microbiol* **106**:760–
584 776. doi:10.1111/mmi.13844

585 Daimon Y, Narita S-I, Miyazaki R, Hizukuri Y, Mori H, Tanaka Y, Tsukazaki T, Akiyama Y. 2020. Reversible
586 autoinhibitory regulation of *Escherichia coli* metallopeptidase BepA for selective β-barrel protein
587 degradation. *Proc Natl Acad Sci U S A* **117**:27989–27996. doi:10.1073/pnas.2010301117

588 Dong H, Xiang Q, Gu Y, Wang Z, Paterson NG, Stansfeld PJ, He C, Zhang Y, Wang W, Dong C. 2014. Structural
589 basis for outer membrane lipopolysaccharide insertion. *Nature* **511**:52–56. doi:10.1038/nature13464

590 Gu Y, Li H, Dong H, Zeng Y, Zhang Z, Paterson NG, Stansfeld PJ, Wang Z, Zhang Y, Wang W, Dong C. 2016.
591 Structural basis of outer membrane protein insertion by the BAM complex. *Nature* **531**:64–69.
592 doi:10.1038/nature17199
593 Gunasinghe SD, Shiota T, Stubenrauch CJ, Schulze KE, Webb CT, Fulcher AJ, Dunstan RA, Hay ID, Naderer T,
594 Whelan DR, Bell TDM, Elgass KD, Strugnell RA, Lithgow T. 2018. The WD40 Protein BamB Mediates
595 Coupling of BAM Complexes into Assembly Precincts in the Bacterial Outer Membrane. *Cell Rep* **23**:2782–
596 2794. doi:10.1016/j.celrep.2018.04.093
597 Han L, Zheng J, Wang Y, Yang X, Liu Y, Sun C, Cao B, Zhou H, Ni D, Lou J, Zhao Y, Huang Y. 2016. Structure
598 of the BAM complex and its implications for biogenesis of outer-membrane proteins. *Nat Struct Mol Biol*
599 **23**:192–196. doi:10.1038/nsmb.3181
600 Hart EM, Gupta M, Wühr M, Silhavy TJ. 2020. The gain-of-function allele *bamA* $_{(E470K)}$ bypasses the essential
601 requirement for BamD in β-barrel outer membrane protein assembly. *Proc Natl Acad Sci U S A* **117**:18737–
602 18743. doi:10.1073/pnas.2007696117
603 Hart EM, Mitchell AM, Konovalova A, Grabowicz M, Sheng J, Han X, Rodriguez-Rivera FP, Schwaid AG,
604 Malinverni JC, Balibar CJ, Bodea S, Si Q, Wang H, Homsher MF, Painter RE, Ogawa AK, Sutterlin H,
605 Roemer T, Black TA, Rothman DM, Walker SS, Silhavy TJ. 2019. A small-molecule inhibitor of BamA
606 impervious to efflux and the outer membrane permeability barrier. *Proc Natl Acad Sci U S A* **116**:21748–
607 21757. doi:10.1073/pnas.1912345116
608 Hizukuri Y, Akiyama Y. 2012. PDZ domains of RseP are not essential for sequential cleavage of RseA or stress-
609 induced σ^E activation *in vivo*. *Mol Microbiol* **86**:1232–1245. doi:10.1111/mmi.12053
610 Iadanza MG, Higgins AJ, Schiffrin B, Calabrese AN, Brockwell DJ, Ashcroft AE, Radford SE, Ranson NA. 2016.
611 Lateral opening in the intact β-barrel assembly machinery captured by cryo-EM. *Nat Commun* **7**:12865.
612 doi:10.1038/ncomms12865
613 Kihara A, Akiyama Y, Ito K. 1995. FtsH is required for proteolytic elimination of uncomplexed forms of SecY,
614 an essential protein translocase subunit. *Proc Natl Acad Sci U S A* **92**:4532–4536.
615 doi:10.1073/pnas.92.10.4532
616 Konovalova A, Kahne DE, Silhavy TJ. 2017. Outer membrane biogenesis. *Annu Rev Microbiol* **71**:539–556.
617 doi:10.1146/annurev-micro-090816-093754

618 Lee J, Sutterlin HA, Wzorek JS, Mandler MD, Hagan CL, Grabowicz M, Tomasek D, May MD, Hart EM, Silhavy
619 TJ, Kahne D. 2018. Substrate binding to BamD triggers a conformational change in BamA to control
620 membrane insertion. *Proc Natl Acad Sci U S A* **115**:2359–2364. doi:10.1073/pnas.1711727115
621 Lee J, Tomasek D, Santos TM, May MD, Meuskens I, Kahne D. 2019. Formation of a β-barrel membrane protein
622 is catalyzed by the interior surface of the assembly machine protein BamA. *eLife* **8**:e49787.
623 doi:10.7554/eLife.49787
624 Lee J, Xue M, Wzorek JS, Wu T, Grabowicz M, Gronenberg LS, Sutterlin HA, Davis RM, Ruiz N, Silhavy TJ,
625 Kahne DE. 2016. Characterization of a stalled complex on the β-barrel assembly machine. *Proc Natl Acad*
626 *Sci U S A* **113**:8717–8722. doi:10.1073/pnas.1604100113
627 López-Pelegrín M, Cerdà-Costa N, Martínez-Jiménez F, Cintas-Pedrola A, Canals A, Peinado JR, Marti-Renom
628 MA, López-Otín C, Arolas JL, Gomis-Rüth FX. 2013. A novel family of soluble minimal scaffolds provides
629 structural insight into the catalytic domains of integral membrane metallopeptidases. *J Biol Chem*
630 **288**:21279–21294. doi:10.1074/jbc.M113.476580
631 Miller JH. 1972. Experiments in Molecular Genetics. Cold Spring Harbor Laboratory Press.
632 Miyazaki R, Akiyama Y, Mori H. 2020a. A photo-cross-linking approach to monitor protein dynamics in living
633 cells. *Biochim Biophys acta Gen Subj* **1864**:129317. doi:10.1016/j.bbagen.2019.03.003
634 Miyazaki R, Akiyama Y, Mori H. 2020b. Fine interaction profiling of VemP and mechanisms responsible for its
635 translocation-coupled arrest-cancelation. *eLife* **9**:e62623. doi:10.7554/eLife.62623
636 Miyazaki R, Myougo N, Mori H, Akiyama Y. 2018. A photo-cross-linking approach to monitor folding and
637 assembly of newly synthesized proteins in a living cell. *J Biol Chem* **293**:677–686.
638 doi:10.1074/jbc.M117.817270
639 Narita S, Masui C, Suzuki T, Dohmae N, Akiyama Y. 2013. Protease homolog BepA (YfgC) promotes assembly
640 and degradation of β-barrel membrane proteins in *Escherichia coli*. *Proc Natl Acad Sci U S A* **110**:E3612–
641 E3621. doi:10.1073/pnas.1312012110
642 Nichols BP, Shafiq O, Meiners V. 1998. Sequence analysis of Tn*10* insertion sites in a collection of *Escherichia*
643 *coli* strains used for genetic mapping and strain construction. *J Bacteriol* **180**:6408–6411.
644 Nikaido H. 2003. Molecular basis of bacterial outer membrane permeability revisited. *Microbiol Mol Biol Rev*
645 **67**:593–656. doi:10.1128/mmbr.67.4.593-656.2003

646 Oh E, Becker AH, Sandikci A, Huber D, Chaba R, Gloge F, Nichols RJ, Typas A, Gross CA, Kramer G, Weissman
647 JS, Bukau B. 2011. Selective ribosome profiling reveals the cotranslational chaperone action of trigger factor
648 in vivo. *Cell* **147**:1295–1308. doi:10.1016/j.cell.2011.10.044
649 Plummer AM, Fleming KG. 2016. From Chaperones to the Membrane with a BAM! *Trends Biochem Sci* **41**:872–
650 882. doi:10.1016/j.tibs.2016.06.005
651 Qiao S, Luo Q, Zhao Y, Zhang XC, Huang Y. 2014. Structural basis for lipopolysaccharide insertion in the
652 bacterial outer membrane. *Nature* **511**:108–111. doi:10.1038/nature13484
653 Rawlings ND, Barrett AJ, Thomas PD, Huang X, Bateman A, Finn RD. 2018. The MEROPS database of
654 proteolytic enzymes, their substrates and inhibitors in 2017 and a comparison with peptidases in the
655 PANTHER database. *Nucleic Acids Res* **46**:D624–D632. doi:10.1093/nar/gkx1134
656 Ricci DP, Silhavy TJ. 2019. Outer membrane protein insertion by the β-barrel assembly machine. *EcoSal Plus*
657 **8**:1–9. doi:10.1128/ecosalplus.ESP-0035-2018
658 Ruiz N, Chng S-S, Hiniker A, Kahne D, Silhavy TJ. 2010. Nonconsecutive disulfide bond formation in an essential
659 integral outer membrane protein. *Proc Natl Acad Sci U S A* **107**:12245–12250.
660 doi:10.1073/pnas.1007319107
661 Ruiz N, Falcone B, Kahne D, Silhavy TJ. 2005. Chemical conditionality: a genetic strategy to probe organelle
662 assembly. *Cell* **121**:307–317. doi:10.1016/j.cell.2005.02.014
663 Schäfer A, Tauch A, Jäger W, Kalinowski J, Thierbach G, Pühler A. 1994. Small mobilizable multi-purpose
664 cloning vectors derived from the *Escherichia coli* plasmids pK18 and pK19: selection of defined deletions
665 in the chromosome of *Corynebacterium glutamicum*. *Gene* **145**:69–73. doi:10.1016/0378-1119(94)90324-7
666 Schwalm J, Mahoney TF, Soltes GR, Silhavy TJ. 2013. Role for Skp in LptD assembly in *Escherichia coli*. *J*
667 *Bacteriol* **195**:3734–3742. doi:10.1128/JB.00431-13
668 Shahrizal M, Daimon Y, Tanaka Y, Hayashi Y, Nakayama S, Iwaki S, Narita S-I, Kamikubo H, Akiyama Y,
669 Tsukazaki T. 2019. Structural basis for the function of the β-barrel assembly-enhancing protease BepA. *J*
670 *Mol Biol* **431**:625–635. doi:10.1016/j.jmb.2018.11.024
671 Soltes GR, Martin NR, Park E, Sutterlin HA, Silhavy TJ. 2017. Distinctive roles for periplasmic proteases in the
672 maintenance of essential outer membrane protein assembly. *J Bacteriol* **199**:e00418-17.
673 doi:10.1128/JB.00418-17

674 Sperandeo P, Martorana AM, Polissi A. 2017. The lipopolysaccharide transport (Lpt) machinery: A
675 nonconventional transporter for lipopolysaccharide assembly at the outer membrane of Gram-negative
676 bacteria. *J Biol Chem* **292**:17981–17990. doi:10.1074/jbc.R117.802512
677 Stöcker W, Bode W. 1995. Structural features of a superfamily of zinc-endopeptidases: the metzincins. *Curr Opin*
678 *Struct Biol* **5**:383–390. doi:10.1016/0959-440x(95)80101-4
679 Tamae C, Liu A, Kim K, Sitz D, Hong J, Becket E, Bui A, Solaimani P, Tran KP, Yang H, Miller JH. 2008.
680 Determination of antibiotic hypersensitivity among 4,000 single-gene-knockout mutants of *Escherichia coli*.
681 *J Bacteriol* **190**:5981–5988. doi:10.1128/JB.01982-07
682 Tomasek D, Kahne D. 2021. The assembly of β-barrel outer membrane proteins. *Curr Opin Microbiol* **60**:16–23.
683 doi:10.1016/j.mib.2021.01.009
684 Tomasek D, Rawson S, Lee J, Wzorek JS, Harrison SC, Li Z, Kahne D. 2020. Structure of a nascent membrane
685 protein as it folds on the BAM complex. *Nature* **583**:473–478. doi:10.1038/s41586-020-2370-1
686 Vertommen D, Ruiz N, Leverrier P, Silhavy TJ, Collet J-F. 2009. Characterization of the role of the *Escherichia*
687 *coli* periplasmic chaperone SurA using differential proteomics. *Proteomics* **9**:2432–2443.
688 doi:10.1002/pmic.200800794
689 Wu T, McCandlish AC, Gronenberg LS, Chng S-S, Silhavy TJ, Kahne D. 2006. Identification of a protein complex
690 that assembles lipopolysaccharide in the outer membrane of *Escherichia coli*. *Proc Natl Acad Sci U S A*
691 **103**:11754–11759. doi:10.1073/pnas.0604744103
692 Yu D, Ellis HM, Lee EC, Jenkins NA, Copeland NG, Court DL. 2000. An efficient recombination system for
693 chromosome engineering in *Escherichia coli. Proc Natl Acad Sci U S A* **97**:5978–5983.
694 doi:10.1073/pnas.100127597
695

Figure 1

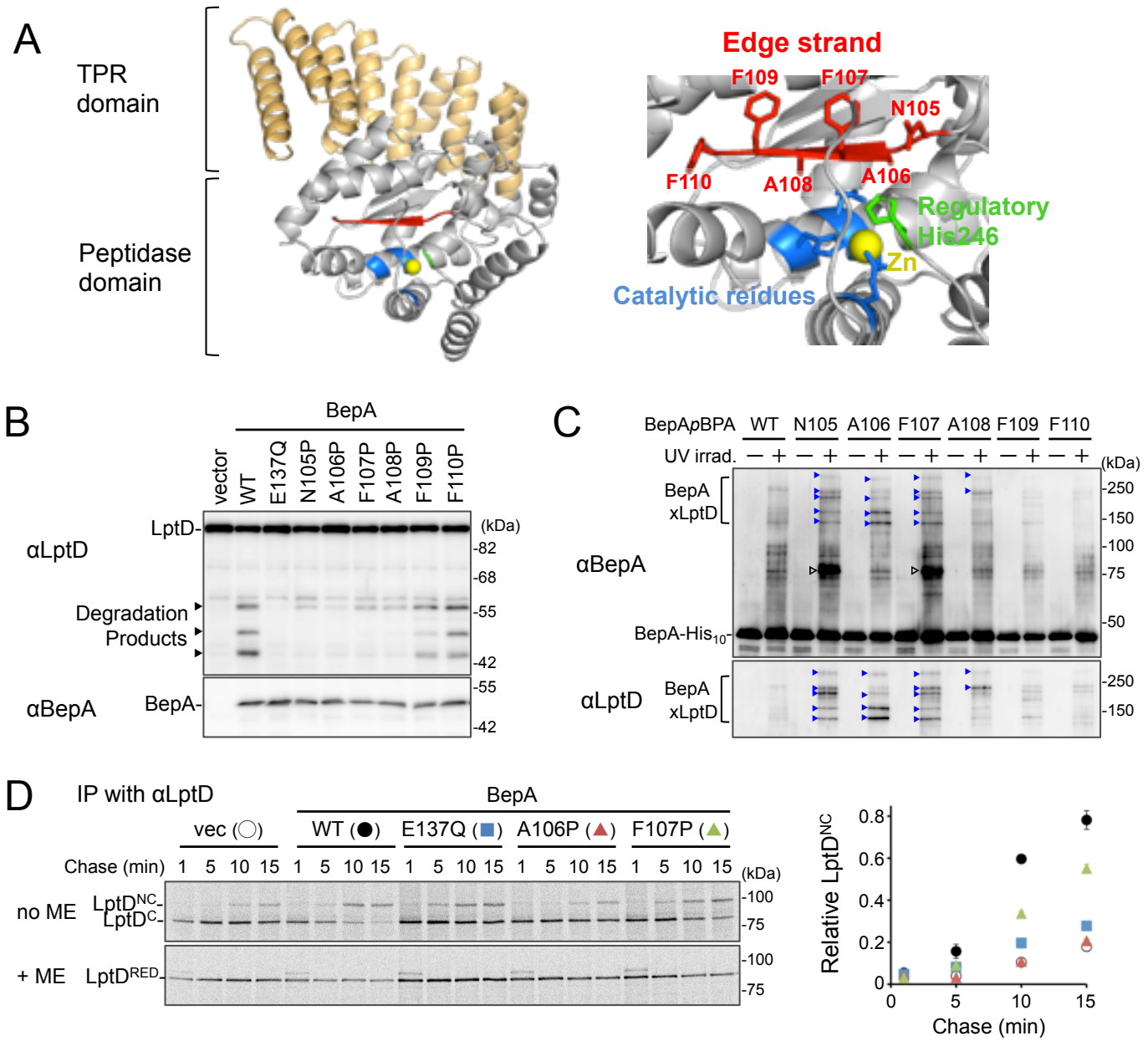

Figure 1. The edge-strand of BepA is crucial for functional interaction with LptD

(**A**) Crystal structure of BepA (PDB code: 6AIT). The peptidase and the TPR domains of BepA are shown in gray and orange, respectively. The edge-strand, the proteolytic active site (the HExxH motif and the third zinc ligand, Glu-201) and the regulatory His-246 residue (His switch) in the peptidase domain are shown in red, blue, and green, respectively, and the coordinated zinc atom is shown in yellow. An enlarged view of the active site region is shown in *right*. (**B**) Protease activities of the BepA edge-strand mutants. Cells of SN56 (Δ*bepA*) carrying pTWV228-*lptD-his*$_{10}$ and either pSTD689 or pSTD689-*bepA* plasmids were grown at 30˚C in L-medium until early log phase and induced with 1 mM IPTG for 1 h. Total cellular proteins were acid-precipitated and analyzed by 7.5 or 10% Laemmli SDS-PAGE and immunoblotting with the indicated antibodies. (**C**) *In vivo* photo-crosslinking analysis of the BepA edge-strand. Cells of SN56 carrying pEVOL-pBpF and pUC18-*bepA(E137Q, amb)-his*$_{10}$ plasmids were grown at 30˚C in L medium containing 0.02% arabinose and 0.5 mM *p*BPA until early log phase, and induced with 1 mM IPTG for 1 h to express the indicated BepA(*p*BPA) variants. The cultures were divided into two portions, each of which was treated with or without UV-irradiation for 10 min at 4˚C. Proteins of the total membrane fractions were subjected to pull-down with Ni-NTA agarose. Purified proteins were analyzed by 7.5% Laemmli SDS-PAGE and immunoblotting with the indicated antibodies. Open triangles indicate unknown crosslinked products. (**D**) Chaperone-like activities of the BepA edge-strand mutants. Cells of SN56 carrying pSTD689 or a pSTD689-*bepA* plasmid were grown at 30˚C in M9-based medium until early log phase, induced with 1 mM IPTG for 15 min, pulse-labeled with ^{35}S-Met for 1 min and chased for the indicated periods. At each time point, total cellular proteins were acid-precipitated, subjected to IP with an anti-LptD antibody, and analyzed by 7.5% Laemmli SDS-PAGE followed by phosphorimaging. The ratio of the band intensities of LptD^{NC} to that of total LptD (LptD^{C} + LptD^{NC}) at the each time point was quantitated and the mean values were plotted with S.D. (n = 2 technical replicates). The result shown is a representative of two independent experiments that were conducted using the same transformants (i.e. two technical replicates).

Figure 2

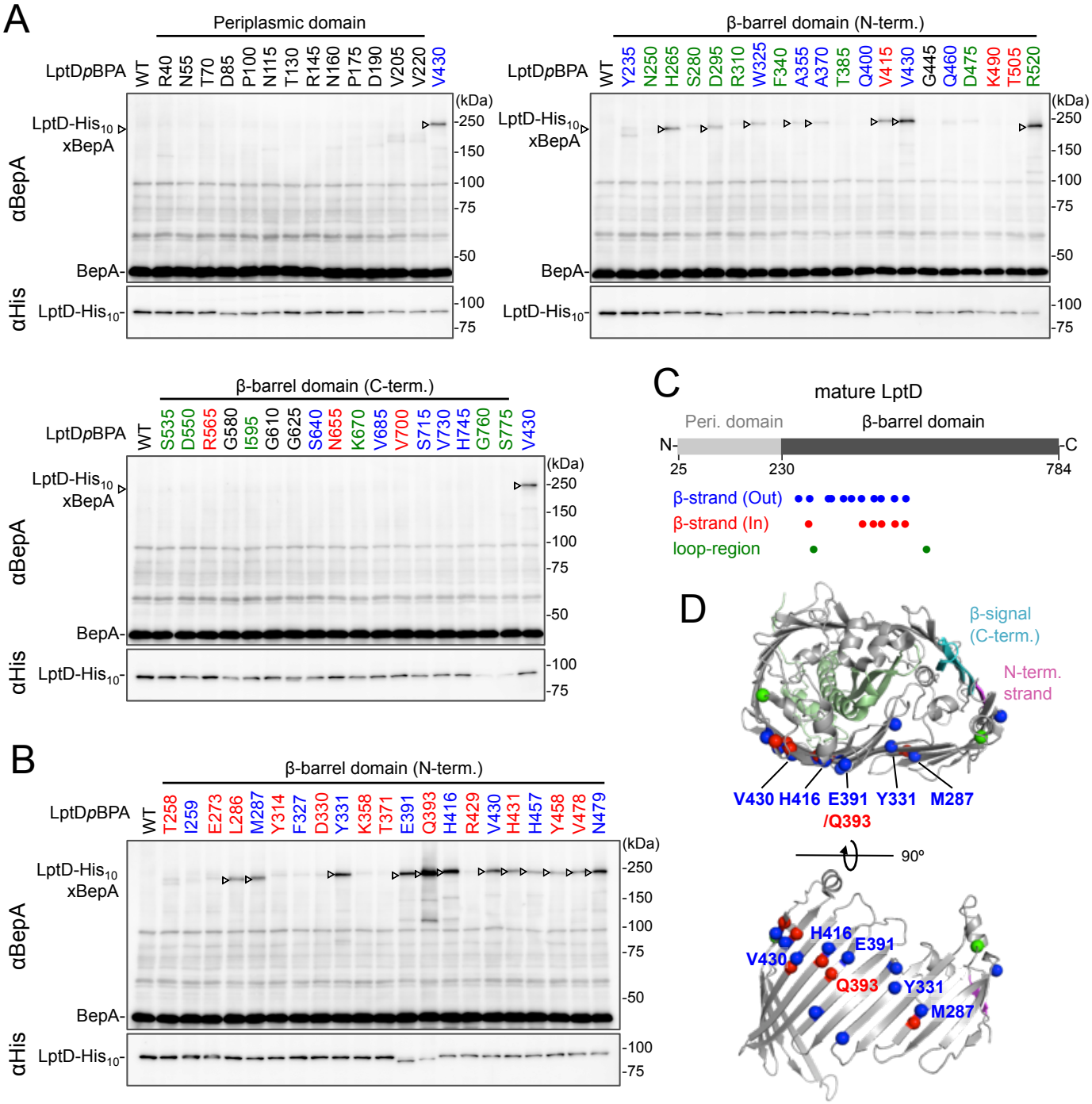

Figure 2. Photo-crosslinking of the the β-barrel forming domain of LptD with BepA

(**A, B**) *In vivo* photo-crosslinking between LptD and BepA. Cells of RM2243 (*bepA(E137Q)*) carrying pEVOL-pBpF, pMW118-*bepA (E137Q, mut)* and pRM294-*lptD(amb)-his*$_{10}$ plasmids were grown at 30˚C in L medium containing 0.02% and 0.5 mM *p*BPA until early log phase and induced with 1 mM IPTG for 3 h to express the indicated LptD(*p*BPA) variants. The cultures were then divided into two portions, each of which was UV-irradiated for 10 min at 4˚C. Total cellular proteins were acid-precipitated and analyzed by 7.5% Laemmli SDS-PAGE and immunoblotting with the indicated antibodies. Most of the LptD mutants were accumulated in comparable amounts. LptD-His$_{10}$xBepA crosslinked products were not detectable with an anti-His antibody due to its low reactivity to LptD-His$_{10}$ in this and the following experiments. Amino acid residues shown in red and blue indicate the ones whose side chain is pointing inward and outward, respectively. Amino acid residues shown in green indicate the ones located in the loop regions. The result shown is a representative of two technical replicates. (**C**) Summary of the BepA crosslinked positions in LptD. Positions where the crosslinking with BepA was clearly and reproducibly detected are indicated by colored dots. (**D**) Mapping of the BepA crosslinked positions on the barrel domain of LptD in the *E. coli* LptD–LptE structure (PDB code: 4RHB). LptD and LptE are shown in gray and light green, respectively. The N-terminal strand and the β-signal (C-terminal region) in the LptD β-barrel domain are shown in magenta and light blue, respectively. The top view of the LptD/E structure from extracellular space (*upper*) and the side view of the N-terminal region of LptD β-domain (*lower*) are shown. The positions where the crosslinking with BepA was observed were indicated by spheres colored as above.

Figure 3

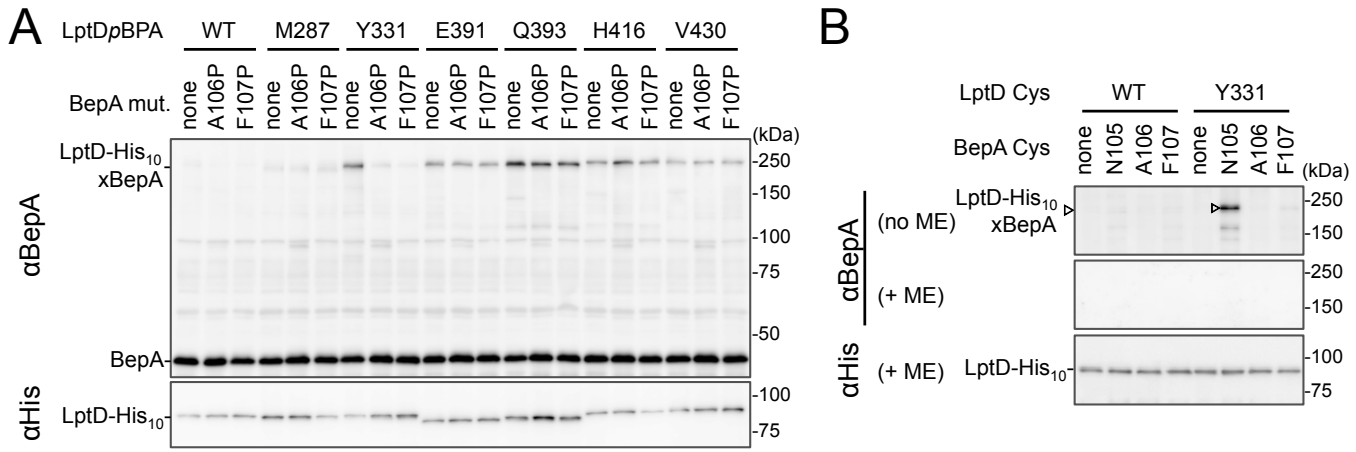

Figure 3. BepA edge-strand directly contacts with the Tyr-331 residue in the N-terminal half region of the LptD β-barrel forming domain

(**A**) Effect of the BepA edge-strand mutations on the crosslinking between BepA and the LptD derivatives having *p*BPA in the N-terminal half region of the LptD b-barrel-forming domain. Cells of SN56 (Δ*bepA*) carrying pEVOL-pBpF, pMW118-*bepA(E137Q, mut)* and pRM294-*lptD(amb)-his$_{10}$* were grown, induced to express a BepA and a LptD*p*BPA derivative and subjected to photo-crosslinking analysis as described in Figure 2. (**B**) Disulfide crosslinking between the Cys residues in the edge-strand of BepA and the N-terminal half region of the LptD β-barrel-forming domain. Cells of SN56 (Δ*bepA*) carrying a combination of plasmids encoding WT or a Cys-introduced mutant of BepA and LptD-His$_{10}$ as indicated were grown in L-medium and induced with 1 mM IPTG for 3 h to express BepA (Cys) and LptD(Cys)-His$_{10}$. Total cellular proteins were acid-precipitated, solubilized with SDS-buffer containing NEM (for blocking free thiol groups) and subjected to pull-down with Ni-NTA agarose. The purified proteins were treated with or without 2-mercaptoethanol (ME) and analyzed by 7.5% Laemmli SDS-PAGE and immunoblotting with the indicated antibodies. The result shown is a representative of two technical replicates.

Figure 4

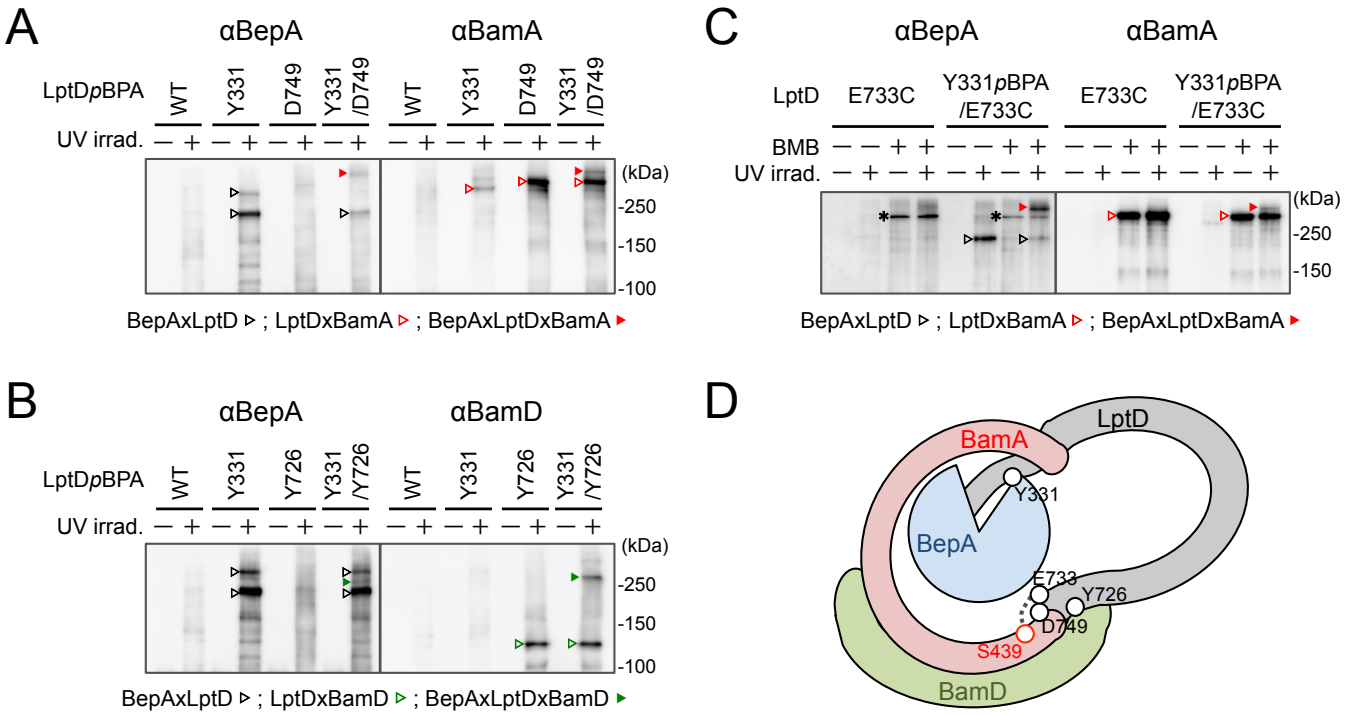

Figure 4. BepA interacts with a LptD intermediate assembling on the BAM complex

(**A, B**) *In vivo* photo-crosslinking of an LptD mutant having *p*BPA at two positions with BepA. Cells of RM2243 (*bepA(E137Q)*) carrying pEVOL-pBpF, pMW118-*bepA(E137Q)* and pRM294-*lptD(amb)-his*$_{10}$ plasmids were grown at 30˚C in L medium containing 0.5 mM *p*BPA until early log phase and induced with 1 mM IPTG for 3 h to express the indicated LptD(*p*BPA) variants. The cultures were divided into two portions, each of which was treated with or without UV-irradiation for 30 min at 4˚C. Proteins of the total membrane fractions were subjected to pull-down with Ni-NTA agarose. Purified proteins were analyzed by 7.5% Laemmli SDS-PAGE by immunoblotting with the indicated antibodies. (**C**) Simultaneous crosslinking of LptD having Y331*p*BPA and E733C with the BepA edge-strand and the seam region of BamA(S439C). Cells of RM3655 (*bamA(S439C)*, Δ*bepA*)/pEVOL-pBpF/pMW118-*bepA(E137Q)* carrying pRM294-*lptD(E733C)-his*$_{10}$ or pRM294-*lptD(Y331amb, E733C)-his*$_{10}$ were grown and induced as in A. After treatment with or without BMB and the following quenching of BMB by addition of excess cysteine, the cultures were divided into two portions, each of which was treated with or without UV-irradiation for 10 min at 4°C. Total cellular proteins were acid-precipitated, solubilized with SDS-buffer containing NEM and subjected to pull-down with Ni-NTA agarose. Purified proteins were analyzed by 7.5% Laemmli SDS-PAGE and immunoblotting with the indicated antibodies. The anti-BamA immunoblotting showed that the amount of the BepAxLptDxBamA crosslinked product was much lower than that of the LptDxBamA crosslinked product. Although the anti-BepA antibodies apparently cross-reacted weakly with the LptDxBamA crosslinked products (asterisks), the higher signal intensity of the BepAxLptDxBamA crosslinked product band as compared with the intensity of the LptDxBamA band indicate that the detection of the former band with the anti-BepA antibodies cannot be ascribed to this cross-reactivity. In **A**–**C**, we confirmed that the amounts of the isolated non-crosslinked LptD-His$_{10}$ derivatives was roughly equal by CBB staining or anti-His immunoblotting (Figure 4-figure supplement 3). The result shown is a representative of two technical replicates. (**D**) A schematic cartoon of the interaction of the LptD assembly intermediate with BepA and BamA/D on the BAM complex.

Figure 5

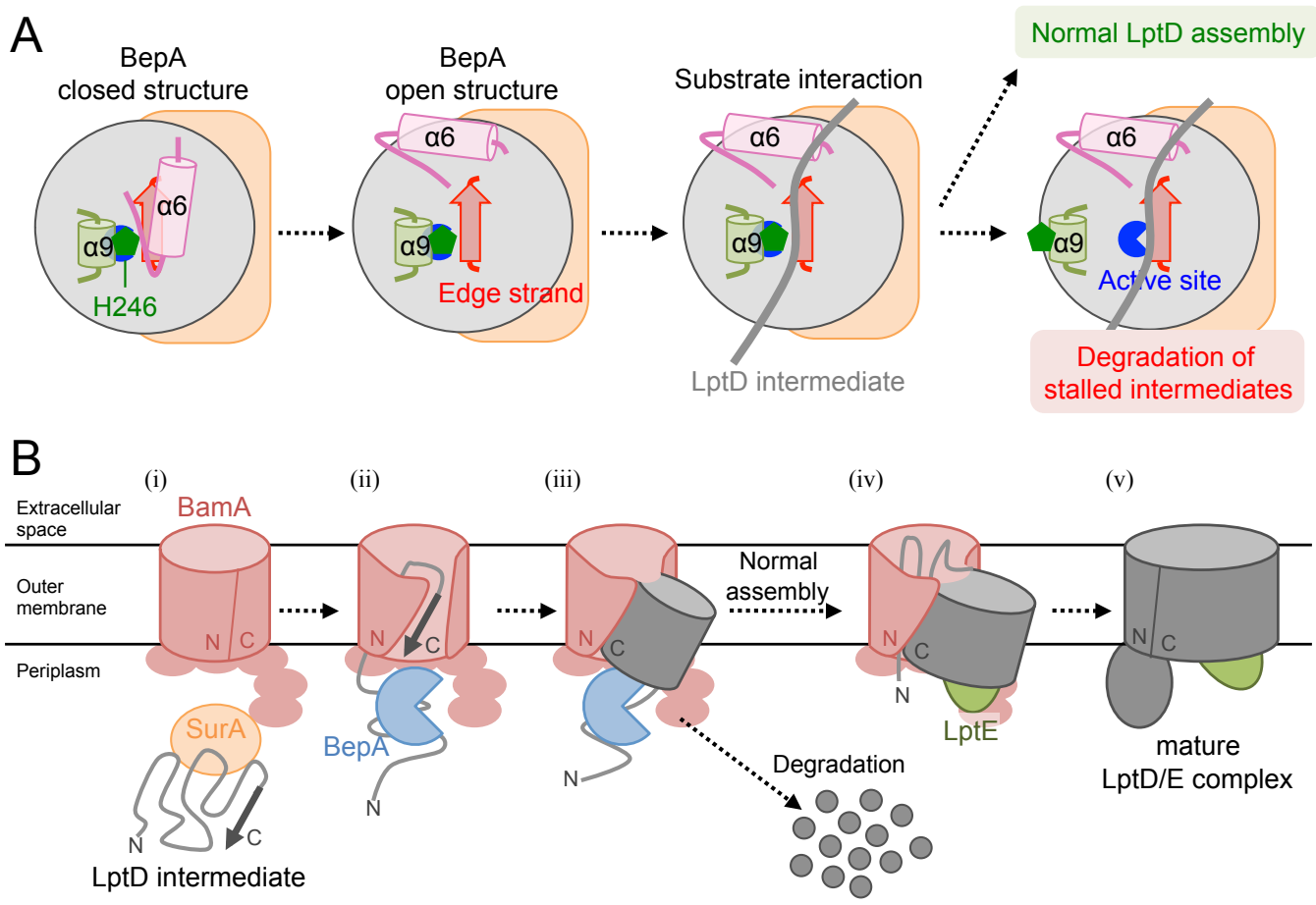

Figure 5. Model for the substrate recognition and discrimination by BepA
(**A**) A schematic cartoon of the substrate recognition by BepA at its active site. See the text for details. (**B**) An overview of the proposed LptD assembly process and BepA-mediated discrimination of the assembling and stalled LptD species. See the text for details.

List of Figure supplements.

Figure 1-figure supplement 1. Sequence alignment of BepA homologs and *E. coli* M48 family peptidases

Figure 1-figure supplement 2. Effects of the BepA edge strand Pro mutations on the BamA degradation and the BepA self-cleavage

Figure 1-figure supplement 3. Functionality of the BepA derivatives having *p*BPA in the edge strand

Figure 1-figure supplement 4. The chaperon-like and proteolytic activities of the BepA edge strand mutants

Figure 2-figure supplement 1. Over-expressed LptD molecules mainly accumulate as $LptD^{C}$

Figure 2-figure supplement 2. Complementation activity of the LptD(*p*BPA) derivatives

Figure 3-figure supplement 1. Effects of the BepA edge strand mutations on the crosslinking of the BepA edge strand to LptD

Figure 3-figure supplement 2. Disulfide crosslinking between BepA and LptD

Figure 4-figure supplement 1. Complementation activity of the LptD derivatives having *p*BPA at one or two positions

Figure 4-figure supplement 3. The amount of affinity purified LptD-His_{10} derivatives

Figure 5-figure supplement 1. α6 and α9-loop regions shield the intramolecular active stie and edge strand of BepA

List of Supplementary files

Supplementary file 1: Table S1. Strains used in this study

Supplementary file 2: Table S2. Plasmids used in this study

Figure 1-figure supplement 1

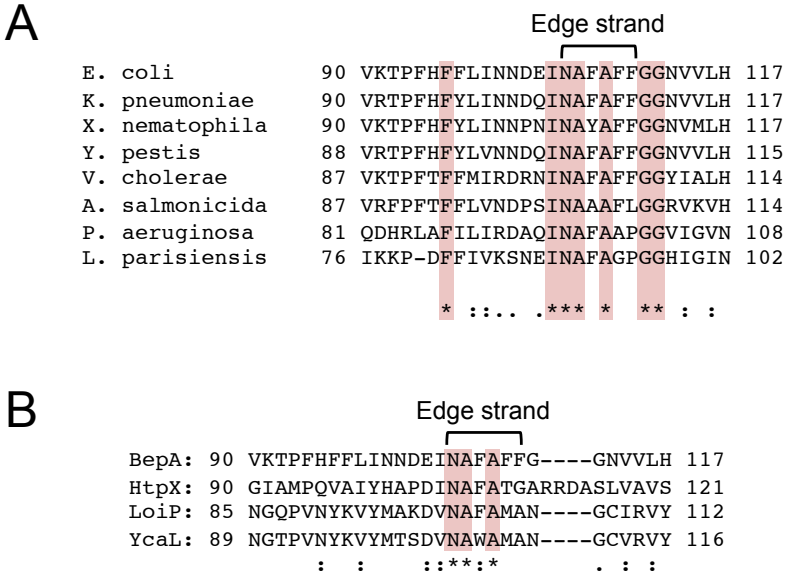

Figure 1-figure supplement 1. Sequence alignment of BepA homologs and *E. coli* M48 family peptidases
(**A**) Alignment of the edge strand amino acid sequences of BepA homologs of *E. coli*, *Klebsiella pneumoniae*, *Xenorhabdus nematophila*, *Yersinia pestis*, *Vibrio cholerae*, *Aeromonas salmonicida*, *Pseudomonas aeruginosa* and *Legionella parisiensis*. (**B**) Alignment of the edge strand amino acid sequences of BepA and other *E. coli* M48 family peptidase (HtpX, LoiP, and YcaL). The alignments were conducted by using the Clustal Omega program. Conserved residues are marked in red.

Figure 1-figure supplement 2

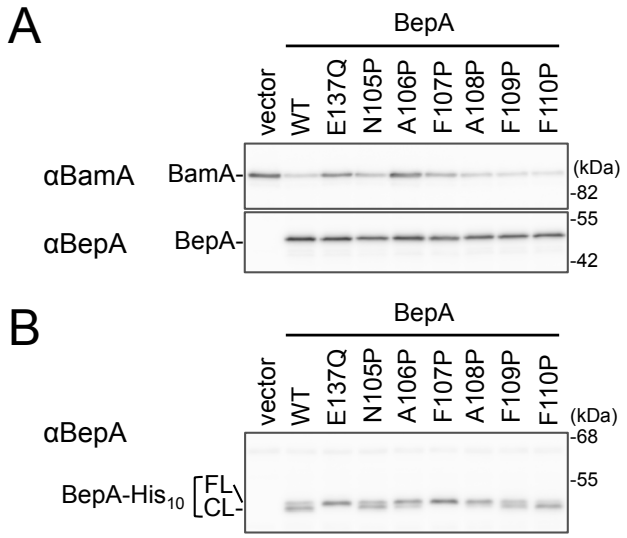

Figure 1-figure supplement 2. Effects of the BepA edge strand Pro mutations on the BamA degradation and the BepA self-cleavage

(**A**) Degradation of BamA in a Δ*surA* strain expressing the BepA edge strand Pro mutants. Cells of SN259 (Δ*bepA*, Δ*surA*) carrying either pSTD689 or pSTD689-*bepA* plasmids were grown at 30˚C in M9-based medium supplemented with 1 mM IPTG for 4 h. Total cellular proteins were acid-precipitated and analyzed by 7.5 or 10% Laemmli SDS-PAGE and immunoblotting with the indicated antibodies. (**B**) C-terminal self-cleavages of the BepA edge strand mutants. Cells of SN56 (Δ*bepA*) carrying either pUC18 or pUC18-*bepA-his*$_{10}$ plasmids were grown at 30˚C in L medium until early log phase and induced with 1 mM IPTG for 1 h. Total cellular proteins were acid-precipitated and analyzed by 7.5% Laemmli SDS-PAGE and immunoblotting with an anti-BepA antibody. The result shown is a representative of two independent experiments that were conducted using the same transformants (i.e. two technical replicates).

Figure 1-figure supplement 3

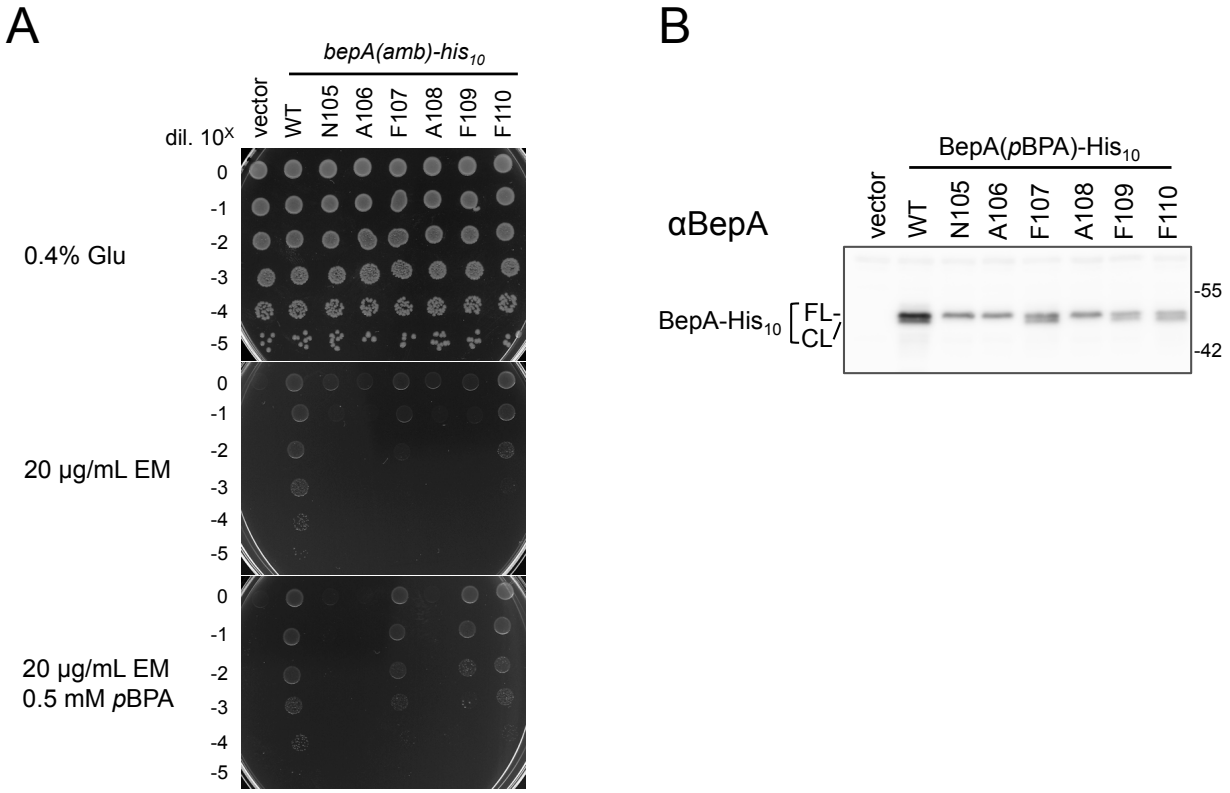

Figure 1-figure supplement 3. Functionality of the BepA derivatives having *p*BPA in the edge strand
(**A**) Complementation activity of the BepA(*p*BPA) derivatives. Cells from 30 μL of overnight cultures of SN56 (Δ*bepA*) carrying pEVOL-pBpF and either pUC18 or pUC18-*bepA(amb)-his*$_{10}$ plasmids were washed, suspended in saline, and serially diluted with saline (to about 10^9 cells/mL). 2.5 μL each of the diluted cells were spotted on L-agar plate or L-agar plates supplemented with 20 μg/mL erythromycin (EM) and 1 mM IPTG with or without 0.5 mM *p*BPA. Plates were incubated at 30˚C for 22 h. (**B**) Self-cleavage of the BepA*p*BPA derivatives. Cells of the same strains in *A* were grown at 30˚C in L medium supplemented with 0.02% arabinose and 0.5 mM *p*BPA until early log phase and induced with 1 mM IPTG for 1 h. Total cellular proteins were acid-precipitated and analyzed by 7.5% Laemmli SDS-PAGE and immunoblotting with an anti-BepA antibody. The result shown is a representative of two technical replicates.

Figure 1-figure supplement 4

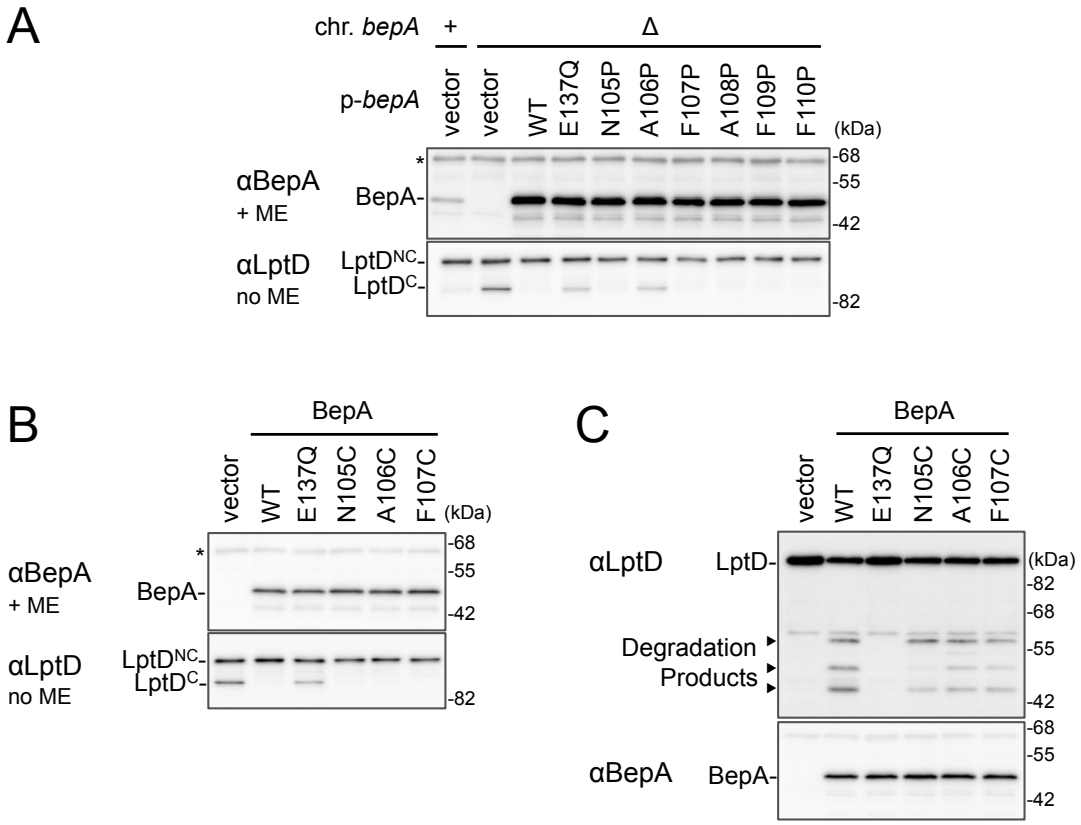

Figure 1-figure supplement 4. The chaperone-like and proteolytic activities of the BepA edge strand mutants
(**A**, **B**) The accumulation of the BepA mutants and LptD^{C} in the Δ*bepA* cells expressing the BepA mutants. Cells of AD16 (*bepA*$^{+}$) carrying pSTD689 (vector) or SN56 (Δ*bepA*) carrying either pSTD689 or pSTD689-*bepA* plasmids were grown at 30˚C in L medium until early log phase and induced with 1 mM IPTG for 1 h. Total cellular proteins were acid-precipitated, and analyzed by 10 or 7.5% Laemmli SDS-PAGE under a reducing (+ME) or non-reducing (no ME) condition and immunoblotting with anti-BepA (*upper* panels) or anti-LptD (*lower* panel) antibodies. (**C**) Protease activities of the BepA edge strand Cys mutants against overproduced LptD. Cells of SN56 (Δ*bepA*) carrying pTWV228-*lptD-his*$_{10}$ and either pSTD689 or pSTD689-*bepA* plasmids were grown at 30˚C in L-medium until early log phase and induced with 1 mM IPTG for 1 h. Total cellular proteins were analyzed as in Figure 1B. The result shown is a representative of two technical replicates.

Figure 2-figure supplement 1

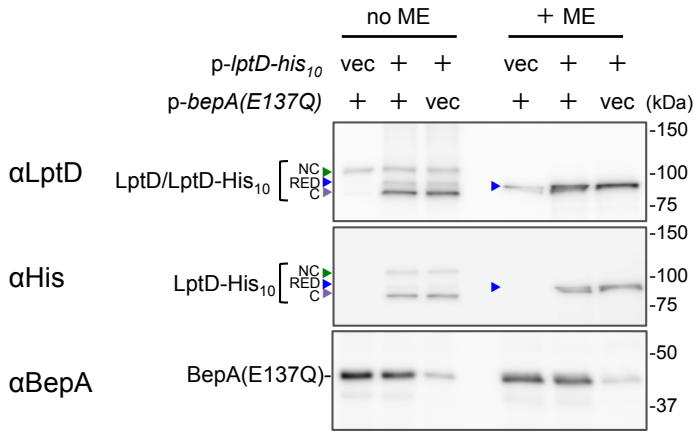

Figure 2-figure supplement 1. Over-expressed LptD molecules mainly accumulate as LptD^{C}
Cells of RM2243(*bepA(E137Q)*)/pEVOL-pBpF carrying either pMW118 or pMW118-*bepA(E137Q)* and either pRM294 or pRM294-*lptD-his$_{10}$* were grown n L medium containing 0.02% arabinose and 0.5 mM *p*BPA until early log phase at 30˚C and induced with 1 mM IPTG for 3 h. Total cellular proteins were acid-precipitated and analyzed by 7.5 or 10% Laemmli SDS-PAGE under a reducing (+ME) or non-reducing (no ME) condition and immunoblotting with the indicated antibodies. The result shown is a representative of two biological replicates.

Figure 2-figure supplement 2

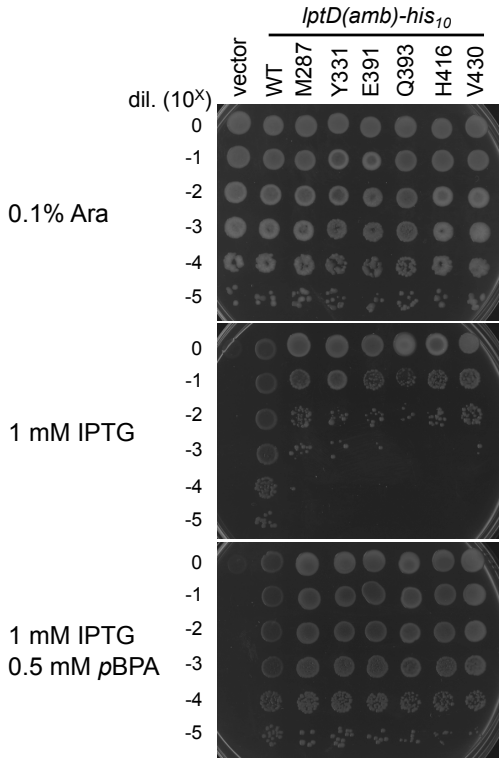

Figure 2-figure supplement 2. Complementation activity of the LptD(*p*BPA) derivatives
Cells of RM3588 (P_{ara}-*lptD*) carrying pEVOL-pBpF and either pRM294 or pRM294-*lptD(amb)-his*$_{10}$ plasmids were grown at 30˚C in L-medium supplemented with 0.1% arabinose for 2.5 h. Cells were washed, suspended in saline, and serially diluted with saline (to about 10^9 cells/mL). 2.5 µL each of the diluted cells were spotted on L-agar plate containing 0.1% arabinose or L medium-based agar plates supplemented with 1 mM IPTG with or without 0.5 mM *p*BPA. Plates were incubated at 30˚C for 22 h. The result shown is a representative of two technical replicates.

Figure 3-figure supplement 1

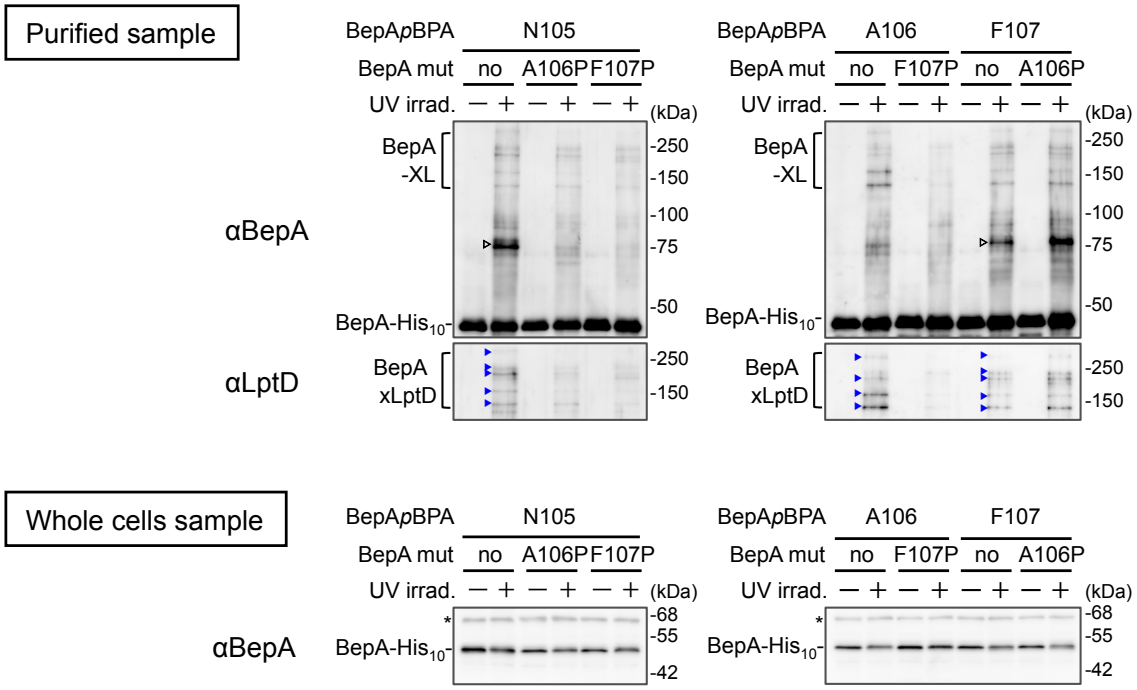

Figure 3-figure supplement 1. Effects of the BepA edge strand mutations on the crosslinking of the BepA edge strand to LptD

Cells SN56 (Δ*bepA*) carrying pEVOL-pBpF and pUC18-*bepA(E137Q, mut., amb)-his*$_{10}$ plasmids were grown in L medium containing 0.02% arabinose and 0.5 mM *p*BPA until early log phase at 30˚C and induced with 1 mM IPTG for 1 h to express the indicated BepA (*p*BPA) variants. The cultures were divided into two portions, each of which was treated with or without UV-irradiation for 10 min at 4˚C. Proteins of the total membrane fractions were subjected to pull-down with Ni-NTA agarose. Purified proteins were analyzed by 7.5% Laemmli SDS-PAGE and immunoblotting with the indicated antibodies. For analysis of the cellular accumulation of each BepA derivative, total cellular proteins of cells of the same cultures were acid-precipitated, and analyzed by 10% Laemmli SDS-PAGE and immunoblotting with the indicated antibodies. Open triangles indicate unknown crosslinked products. The result shown is a representative of two technical replicates.

Figure 3-figure supplement 2

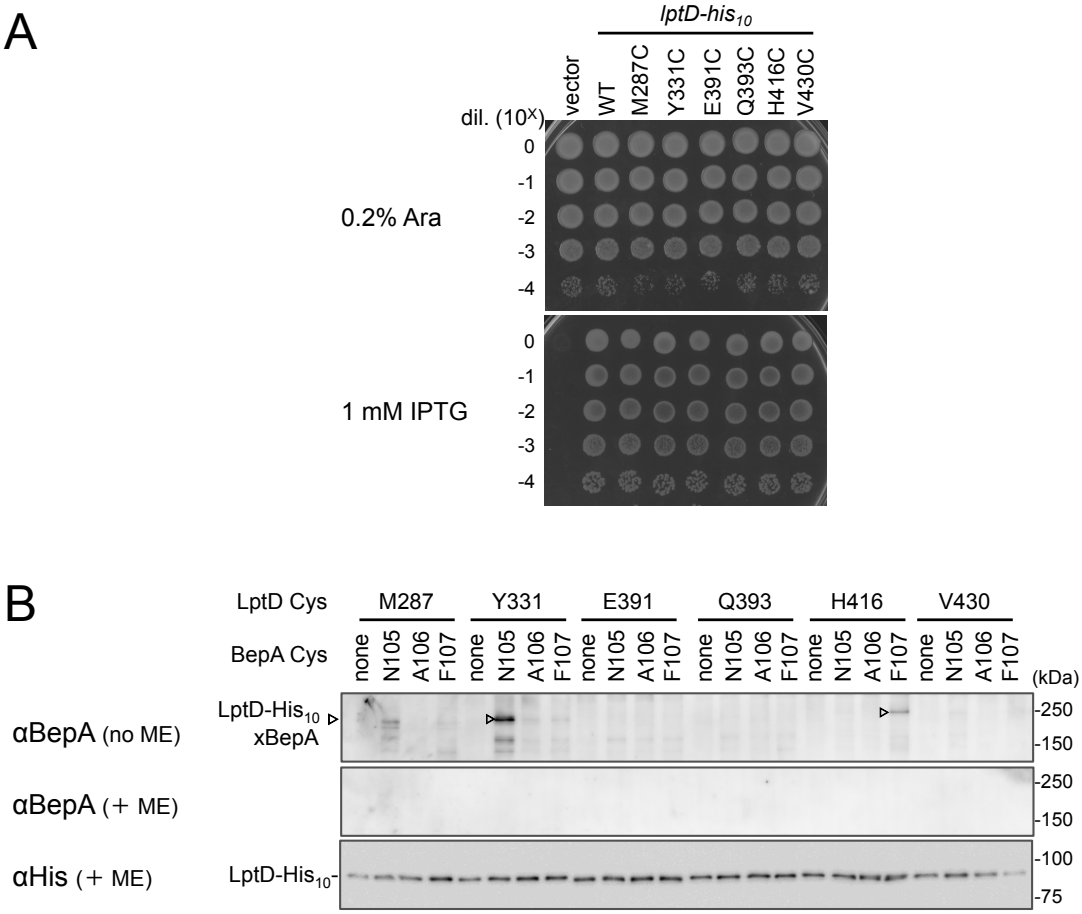

Figure 3-figure supplement 2. Disulfide crosslinking between BepA and LptD

(**A**) Complementation activity of the LptD derivatives with an engineered Cys residue. Cells of RM3588 (P_{ara}-*lptD*) carrying pRM294 or pRM294-*lptD(Cys)-his*$_{10}$ plasmids were grown at 30˚C in L medium supplemented with 0.1% arabinose for 2.5 h. Cells were washed, suspended in saline, and serially diluted with saline (to about 10^9 cells/mL). 2.5 µL each of the diluted cells were spotted on L-agar plate containing 0.1% arabinose or 1 mM IPTG. Plates were incubated at 30˚C for 22 h. (**B**) BepA–LptD disulfide crosslinking. Cells of SN56 (Δ*bepA*) carrying a combination of plasmids encoding WT or a Cys-mutant form of BepA and LptD-His$_{10}$ as indicated were grown in L-medium and induced with 1 mM IPTG for 3 h to express BepA(Cys) and LptD(Cys)-His$_{10}$. Total cellular proteins were acid-precipitated, solubilized with SDS buffer containing NEM and subjected to pull-down with Ni-NTA agarose. The purified proteins were treated with or without 2-mercaptoethanol (ME) and analyzed by 7.5% Laemmli SDS-PAGE and immunoblotting with the indicated antibodies. The result shown is a representative of two technical replicates.

Figure 4-figure supplement 1

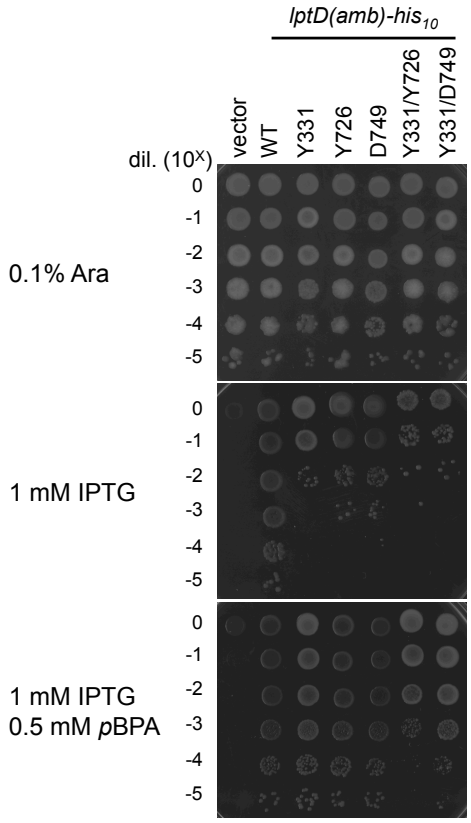

Figure 4-figure supplement 1. Complementation activity of the LptD derivatives having *p*BPA at one or two positions

Cells of RM3588 (P_{ara}-*lptD*) carrying pEVOL-pBpF and either pRM294 or pRM294-*lptD(amb)-his*$_{10}$ plasmids were grown and analyzed as in Figure 2-figure supplement 2. The result shown is a representative of two technical replicates.

Figure 4-figure supplement 2

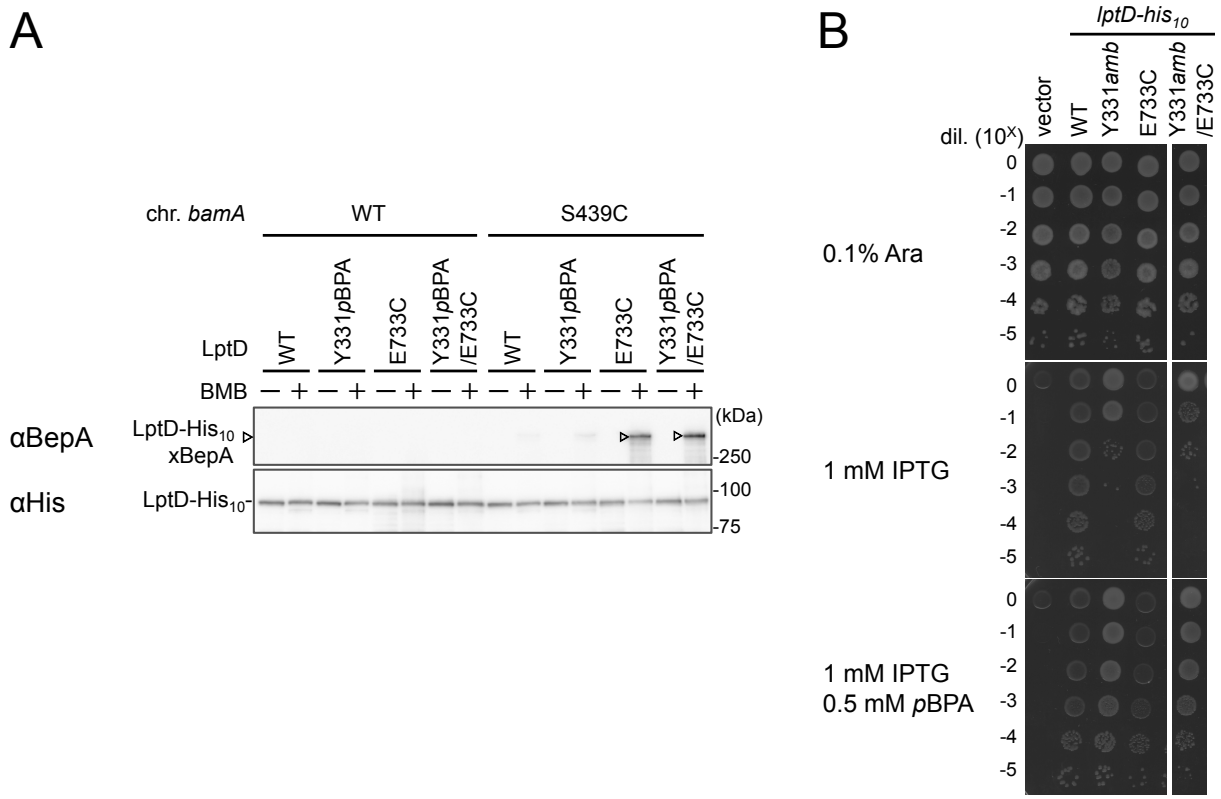

Figure 4-figure supplement 2. BMB crosslinking between LptD(Y331*p*BPA/E733C) and BamA(S439C)
(**A**) BMB crosslinking. Cells of RM3654 (*bamA*$^+$, Δ*bepA*)/pEVOL-pBpF/pMW118-*bepA(E137Q)* or RM3655 (*bamA(S439C)*, Δ*bepA*)/ pEVOL-pBpF/pMW118-*bepA(E137Q)* carrying each pRM294-*lptD-his*$_{10}$ derivative were grown at 30˚C in L medium containing 0.5 mM *p*BPA until early log phase and induced with 1 mM IPTG for 3 h to express the indicated LptD variants. Cell cultures were treated with TCEP to reduce possible artificially-formed disulfide bonds for E733C in LptD and S439C in BamA. The cultures were divided into two portions, each of which was treated with or without BMB. After quenching of BMB by addition of excess cysteine, total cellular proteins were acid-precipitated, solubilized with SDS-buffer containing NEM and subjected to pull-down with Ni-NTA agarose. The purified proteins were analyzed by 7.5% Laemmli SDS-PAGE and immunoblotting with the indicated antibodies. (**B**) Complementation activity of LptD derivatives. Cells of RM3588 (P_{ara}-*lptD*) carrying pEVOL-pBpF and pRM294 or each pRM294-*lptD-his*$_{10}$ derivative were grown are analyzed as in Figure 2-figure supplement 2. The result shown is a representative of two technical replicates.

Figure 4-figure supplement 3

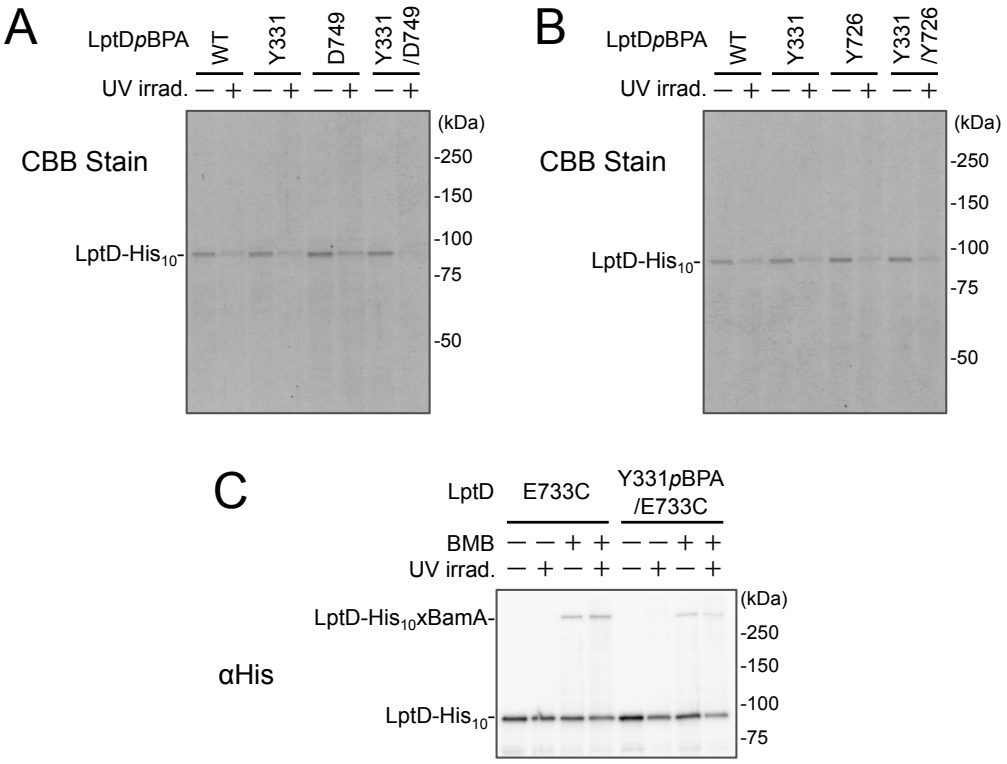

Figure 4-figure supplement 3. The amount of affinity purified LptD-His$_{10}$ derivatives
Affinity isolated proteins in Figure 4A-C were separated by 7.5% Laemmli SDS-PAGE and subjected to CBB staining (**A** and **B** for Figure 4A and B, respectively) or anti-His immunoblotting (**C** for Figure 4C). The result shown is a representative of two technical replicates.

Figure 5-figure supplement 1

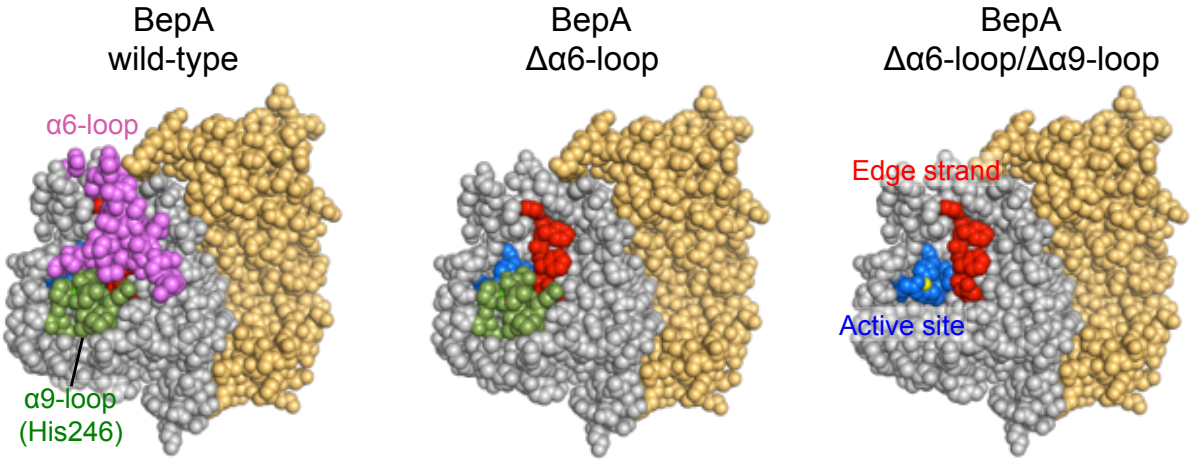

Figure 5-figure supplement 1. α6 and α9-loop regions shield the intramolecular active stie and edge strand of BepA
The space-filling models of wild type BepA (*left*), BepA without the α6-loop (*middle*) and BepA without the α6- and α9-loops (*right*). The peptidase and the TPR domains of the BepA crystal structure (PDB code: 6AIT) are shown in gray and orange, respectively. The α6-loop, the α9-loop, the proteolytic active site (the HExxH motif and the third zinc ligand, Glu-201) and the edge strand in the peptidase domain are shown in magenta, green, blue and red, respectively.

Table S1. Strains used in this study

Strain	Genotype	References
AD16	Δ*pro-lac thi*/F' *lacI*^{q} *Z*Δ*M15 Y*$^+$ *pro*$^+$	(Kihara et al., 1995)
SN56	AD16, Δ*bepA*	(Narita et al., 2013)
SN259	AD16, Δ*bepA ΔsurA*::*kan*	(Narita et al., 2013)
RM2243	AD16, *bepA(E137Q) purC80*::Tn*10*	This study
RM3654	AD16, Δ*bepA bamA*$^+$ *zae502*::Tn*10*	This study
RM3655	AD16, Δ*bepA bamA(S439C) zae502*::Tn*10*	This study
JE6631	*Hfr:str thi polA1*	(Mori et al., 2002)
RM2091	JE6631, *purC80*::Tn*10*	This study
YH188	JE6631, *zae502*::Tn*10*	(Hizukuri and Akiyama, 2012)
MC4100	F$^-$ *araD139* Δ*(argF-lac)U169 rpsL150 relA1 flbB5301 deoC1 ptsF25 rbsR*	(Casadaban, 1976)
CU141	MC4100/F' *lacI*^{q} *lacZ*$^+$, *Y*$^+$, *A*$^+$	(Akiyama et al., 1994)
HM1742	CU141 *ara*$^+$	(Mori and Ito, 2006)
RM3588	HM1742, *kan araC*-P$_{araBAD}$-*lptD*	This study
DY330	W3110, Δ*lacU169 gal490 λcI857* Δ(*cro-bioA*)	(Yu et al., 2000)
RM3444	DY330, *kan araC*-P$_{araBAD}$-*lptD*	This study

(References)

Akiyama Y, Ogura T, Ito K. 1994. Involvement of FtsH in protein assembly into and through the membrane. I. Mutations that reduce retention efficiency of a cytoplasmic reporter. *J Biol Chem* **269**:5218–5224. doi:10.1016/S0021-9258(17)37677-9

Casadaban MJ. 1976. Transposition and fusion of the *lac* genes to selected promoters in *Escherichia coli* using bacteriophage lambda and Mu. *J Mol Biol* **104**:541–555. doi:10.1016/0022-2836(76)90119-4

Hizukuri Y, Akiyama Y. 2012. PDZ domains of RseP are not essential for sequential cleavage of RseA or stress-induced σ^E activation *in vivo*. *Mol Microbiol* **86**:1232–1245. doi:10.1111/mmi.12053

Kihara A, Akiyama Y, Ito K. 1995. FtsH is required for proteolytic elimination of uncomplexed forms of SecY, an essential protein translocase subunit. *Proc Natl Acad Sci U S A* **92**:4532–4536. doi:10.1073/pnas.92.10.4532

Mori H, Ito K. 2006. The long α-helix of SecA is important for the ATPase coupling of translocation. *J Biol Chem* **281**:36249–36256. doi:10.1074/jbc.M606906200

Mori H, Shimizu Y, Ito K. 2002. Superactive SecY variants that fulfill the essential translocation function with a reduced cellular quantity. *J Biol Chem* **277**:48550–48557. doi:10.1074/jbc.M204436200

Narita S, Masui C, Suzuki T, Dohmae N, Akiyama Y. 2013. Protease homolog BepA (YfgC) promotes assembly and degradation of β-barrel membrane proteins in *Escherichia coli*. *Proc Natl Acad Sci U S A* **110**:E3612–E3621. doi:10.1073/pnas.1312012110

Yu D, Ellis HM, Lee EC, Jenkins NA, Copeland NG, Court DL. 2000. An efficient recombination system for chromosome engineering in *Escherichia coli. Proc Natl Acad Sci U S A* **97**:5978–5983. doi:10.1073/pnas.100127597

Table S2. Plasmids used in this study

Plasmid	Vector	Encoded protein and description	Reference or source
pEVOL-pBpF		p15A-derivative encoding an evolved *M. jannaschii* aminoacyl-tRNA synthetase/ suppressor tRNA pair for incorporation of *p*BPA; CmR	(Young et al., 2010)
pSTD689		pACYC184-derived expression vector; P_{lac}, Spc^R	(Kanehara et al., 2003)
pRM290	pSTD689	BepA	(Daimon et al., 2017)
pRM291	pSTD689	BepA(E137Q)	(Daimon et al., 2017)
pRM512	pSTD689	BepA(N105P)	This study
pRM513	pSTD689	BepA(A106P)	This study
pRM514	pSTD689	BepA(F107P)	This study
pRM515	pSTD689	BepA(A108P)	This study
pRM516	pSTD689	BepA(F109P)	This study
pRM517	pSTD689	BepA(F110P)	This study
pRM833	pSTD689	BepA(N105C)	This study
pRM786	pSTD689	BepA(N105C, E137Q)	This study
pRM834	pSTD689	BepA(A106C)	This study
pRM787	pSTD689	BepA(A106C, E137Q)	This study
pRM835	pSTD689	BepA(F107C)	This study
pRM788	pSTD689	BepA(F107C, E137Q)	This study
pUC18		Expression vector; P_{lac}, Amp^R	Takara Bio
pUC-bepA(E137Q)	pUC18	BepA(E137Q)	(Narita et al., 2013)
pUC-bepA-his_{10}	pUC18	BepA-His_{10}	(Narita et al., 2013)
pUC-bepA(E137Q)-his_{10}	pUC18	BepA(E137Q)-His_{10}	(Narita et al., 2013)
pYN333	pUC18	BepA(N105P)-His_{10}	This study
pYN334	pUC18	BepA(A106P)-His_{10}	This study
pYN335	pUC18	BepA(F107P)-His_{10}	This study
pYN336	pUC18	BepA(A108P)-His_{10}	This study
pYN337	pUC18	BepA(F109P)-His_{10}	This study
pYN338	pUC18	BepA(F110P)-His_{10}	This study
pYN339	pUC18	BepA(N105*amb*)-His_{10}	This study
pRM536	pUC18	BepA(N105*amb*, E137Q)-His_{10}	This study
pRM778	pUC18	BepA(N105*amb*, A106P, E137Q)-His_{10}	This study
pRM779	pUC18	BepA(N105*amb*, F107P, E137Q)-His_{10}	This study
pYN340	pUC18	BepA(A106*amb*)-His_{10}	This study
pRM537	pUC18	BepA(A106*amb*, E137Q)-His_{10}	This study
pYN345	pUC18	BepA(A106*amb*, F107P, E137Q)-His_{10}	This study
pYN341	pUC18	BepA(F107*amb*)-His_{10}	This study
pRM538	pUC18	BepA(F107*amb*, E137Q)-His_{10}	This study

pYN346	pUC18	BepA(F107*amb*, A106P, E137Q)-His_{10}	This study
pYN342	pUC18	BepA(A108*amb*)-His_{10}	This study
pRM539	pUC18	BepA(A108*amb*, E137Q)-His_{10}	This study
pYN343	pUC18	BepA(F109*amb*)-His_{10}	This study
pRM540	pUC18	BepA(F109*amb*, E137Q)-His_{10}	This study
pYN344	pUC18	BepA(F110*amb*)-His_{10}	This study
pRM541	pUC18	BepA(F110*amb*, E137Q)-His_{10}	This study
pMW118		pSC101-derived expression vector; P_{lac}, Amp^R	Nippon Gene
pNB91	pMW118	BepA(E137Q)	This study
pRM807	pMW118	BepA(A106P, E137Q)	This study
pRM808	pMW118	BepA(F107P, E137Q)	This study
pTWV228		pBR322-derived expression vector; P_{lac}, Amp^R	Takara Bio
pRM267	pTWV228	LptD-His_{10} (using the native SD sequence)	(Daimon et al., 2017)
pRM816	pTWV228	LptD-His_{10}^{SD} (using a strong SD sequence)	This study
pRM810	pTWV228	LptD(M287C)-His_{10}^{SD}	This study
pRM811	pTWV228	LptD(Y331C)-His_{10}^{SD}	This study
pRM812	pTWV228	LptD(E391C)-His_{10}^{SD}	This study
pRM813	pTWV228	LptD(Q393C)-His_{10}^{SD}	This study
pRM814	pTWV228	LptD(H416C)-His_{10}^{SD}	This study
pRM815	pTWV228	LptD(V430C)-His_{10}^{SD}	This study
pRM294		pBR322-derived expression vector; P_{lac}, Spc^R	(Miyazaki et al., 2018)
pRM309	pRM294	LptD-His_{10}^{SD} (using a strong SD sequence)	(Miyazaki et al., 2018)
pNB22	pRM294	LptD(R40*amb*)-His_{10}^{SD}	This study
pNB23	pRM294	LptD(N55*amb*)-His_{10}^{SD}	This study
pNB24	pRM294	LptD(T70*amb*)-His_{10}^{SD}	This study
pNB25	pRM294	LptD(D85*amb*)-His_{10}^{SD}	This study
pNB26	pRM294	LptD(P100*amb*)-His_{10}^{SD}	This study
pNB27	pRM294	LptD(N115*amb*)-His_{10}^{SD}	This study
pNB28	pRM294	LptD(T130*amb*)-His_{10}^{SD}	This study
pNB29	pRM294	LptD(R145*amb*)-His_{10}^{SD}	This study
pNB30	pRM294	LptD(N160*amb*)-His_{10}^{SD}	This study
pNB31	pRM294	LptD(P175*amb*)-His_{10}^{SD}	This study
pNB49	pRM294	LptD(D190*amb*)-His_{10}^{SD}	This study
pNB50	pRM294	LptD(V205*amb*)-His_{10}^{SD}	This study
pNB51	pRM294	LptD(V220*amb*)-His_{10}^{SD}	This study
pNB52	pRM294	LptD(Y235*amb*)-His_{10}^{SD}	This study
pNB53	pRM294	LptD(N250*amb*)-His_{10}^{SD}	This study
pRM618	pRM294	LptD(T258*amb*)-His_{10}^{SD}	This study
pRM619	pRM294	LptD(I259*amb*)-His_{10}^{SD}	This study

pNB54	pRM294	LptD(H265*amb*)-His_{10}^{SD}	This study
pRM620	pRM294	LptD(E273*amb*)-His_{10}^{SD}	This study
pNB55	pRM294	LptD(S280*amb*)-His_{10}^{SD}	This study
pRM621	pRM294	LptD(L286*amb*)-His_{10}^{SD}	This study
pRM622	pRM294	LptD(M287*amb*)-His_{10}^{SD}	This study
pNB56	pRM294	LptD(S295*amb*)-His_{10}^{SD}	This study
pNB57	pRM294	LptD(R310*amb*)-His_{10}^{SD}	This study
pRM623	pRM294	LptD(Y314*amb*)-His_{10}^{SD}	This study
pNB58	pRM294	LptD(W325*amb*)-His_{10}^{SD}	This study
pRM624	pRM294	LptD(F327*amb*)-His_{10}^{SD}	This study
pRM625	pRM294	LptD(D330*amb*)-His_{10}^{SD}	This study
pRM626	pRM294	LptD(Y331*amb*)-His_{10}^{SD}	This study
pNB59	pRM294	LptD(F340*amb*)-His_{10}^{SD}	This study
pNB60	pRM294	LptD(A355*amb*)-His_{10}^{SD}	This study
pRM627	pRM294	LptD(K358*amb*)-His_{10}^{SD}	This study
pNB61	pRM294	LptD(A370*amb*)-His_{10}^{SD}	This study
pRM628	pRM294	LptD(T371*amb*)-His_{10}^{SD}	This study
pNB62	pRM294	LptD(T385*amb*)-His_{10}^{SD}	This study
pRM629	pRM294	LptD(E391*amb*)-His_{10}^{SD}	This study
pRM630	pRM294	LptD(Q393*amb*)-His_{10}^{SD}	This study
pNB63	pRM294	LptD(Q400*amb*)-His_{10}^{SD}	This study
pNB64	pRM294	LptD(V415*amb*)-His_{10}^{SD}	This study
pRM631	pRM294	LptD(H416*amb*)-His_{10}^{SD}	This study
pRM632	pRM294	LptD(R429*amb*)-His_{10}^{SD}	This study
pNB65	pRM294	LptD(V430*amb*)-His_{10}^{SD}	This study
pRM633	pRM294	LptD(H431*amb*)-His_{10}^{SD}	This study
pNB66	pRM294	LptD(G445*amb*)-His_{10}^{SD}	This study
pRM634	pRM294	LptD(H457*amb*)-His_{10}^{SD}	This study
pRM635	pRM294	LptD(Y458*amb*)-His_{10}^{SD}	This study
pNB67	pRM294	LptD(Q460*amb*)-His_{10}^{SD}	This study
pNB68	pRM294	LptD(D475*amb*)-His_{10}^{SD}	This study
pRM636	pRM294	LptD(V478*amb*)-His_{10}^{SD}	This study
pRM637	pRM294	LptD(N479*amb*)-His_{10}^{SD}	This study
pNB69	pRM294	LptD(K490*amb*)-His_{10}^{SD}	This study
pNB70	pRM294	LptD(T505*amb*)-His_{10}^{SD}	This study
pNB71	pRM294	LptD(R520*amb*)-His_{10}^{SD}	This study
pNB72	pRM294	LptD(S535*amb*)-His_{10}^{SD}	This study
pNB73	pRM294	LptD(D550*amb*)-His_{10}^{SD}	This study
pNB74	pRM294	LptD(R565*amb*)-His_{10}^{SD}	This study
pNB75	pRM294	LptD(G580*amb*)-His_{10}^{SD}	This study

pNB76	pRM294	LptD(I595*amb*)-His_{10}^{SD}	This study
pNB77	pRM294	LptD(G610*amb*)-His_{10}^{SD}	This study
pNB78	pRM294	LptD(G625*amb*)-His_{10}^{SD}	This study
pNB79	pRM294	LptD(S640*amb*)-His_{10}^{SD}	This study
pNB80	pRM294	LptD(N655*amb*)-His_{10}^{SD}	This study
pNB81	pRM294	LptD(K670*amb*)-His_{10}^{SD}	This study
pNB82	pRM294	LptD(V685*amb*)-His_{10}^{SD}	This study
pNB83	pRM294	LptD(V700*amb*)-His_{10}^{SD}	This study
pNB84	pRM294	LptD(S715*amb*)-His_{10}^{SD}	This study
pNB32	pRM294	LptD(Y726*amb*)-His_{10}^{SD}	This study
pNB85	pRM294	LptD(V730*amb*)-His_{10}^{SD}	This study
pNB86	pRM294	LptD(H745*amb*)-His_{10}^{SD}	This study
pRM809	pRM294	LptD(D749*amb*)-His_{10}^{SD}	This study
pNB87	pRM294	LptD(G760*amb*)-His_{10}^{SD}	This study
pNB88	pRM294	LptD(S775*amb*)-His_{10}^{SD}	This study
pRM821	pRM294	LptD(Y331*amb*, D749*amb*)-His_{10}^{SD}	This study
pRM822	pRM294	LptD(Y331*amb*, Y726*amb*)-His_{10}^{SD}	This study
pRM829	pRM294	LptD(E733C)-His_{10}^{SD}	This study
pRM831	pRM294	LptD(Y331*amb*, E733C)-His_{10}^{SD}	This study
pUC118		Expression vector; P_{lac}, Amp^R	Takara Bio
pRM320	pUC118	*bepA-yfgD*	This study
pRM324	pUC118	*bepA(E137Q)-yfgD*	This study
pRM823	pUC118	*bamA*	This study
pRM836	pUC118	*bamA(S439C)*	This study
pK18mobsacB		pBR322-derived vector carrying *sacB* for chromosomal gene replacement; Km^R	(Schäfer et al., 1994)
pRM330	pK18mobsacB	*bepA(E137Q)-yfgD*	This study
pRM845	pK18mobsacB	*bamA(S439C)*	This study

(References)

Daimon Y, Iwama-Masui C, Tanaka Y, Shiota T, Suzuki T, Miyazaki R, Sakurada H, Lithgow T, Dohmae N, Mori H, Tsukazaki T, Narita S-I, Akiyama Y. 2017. The TPR domain of BepA is required for productive interaction with substrate proteins and the β-barrel assembly machinery complex. *Mol Microbiol* **106**:760–776. doi:10.1111/mmi.13844

Kanehara K, Ito K, Akiyama Y. 2003. YaeL proteolysis of RseA is controlled by the PDZ domain of YaeL and a Gln-rich region of RseA. *EMBO J* **22**:6389–6398. doi:10.1093/emboj/cdg602

Miyazaki R, Myougo N, Mori H, Akiyama Y. 2018. A photo-cross-linking approach to monitor folding and assembly of newly synthesized proteins in a living cell. *J Biol Chem* **293**:677–686. doi:10.1074/jbc.M117.817270

Narita S, Masui C, Suzuki T, Dohmae N, Akiyama Y. 2013. Protease homolog BepA (YfgC) promotes assembly and degradation of β-barrel membrane proteins in *Escherichia coli*. *Proc Natl Acad Sci U S A* **110**:E3612–E3621. doi:10.1073/pnas.1312012110

Schäfer A, Tauch A, Jäger W, Kalinowski J, Thierbach G, Pühler A. 1994. Small mobilizable multi-purpose cloning vectors derived from the *Escherichia coli* plasmids pK18 and pK19: selection of defined deletions in the chromosome of *Corynebacterium glutamicum*. *Gene* **145**:69–73. doi:10.1016/0378-1119(94)90324-7

Young TS, Ahmad I, Yin JA, Schultz PG. 2010. An enhanced system for unnatural amino acid mutagenesis in *E. coli*. *J Mol Biol* **395**:361–374. doi:10.1016/j.jmb.2009.10.030